

Quantum Coherence in Electrical Circuits

by

Jeyran Amirloo Abolfathi

A thesis
presented to the University of Waterloo
in fulfillment of the
thesis requirement for the degree of
Master of Applied Science
in
Electrical and Computer Engineering

Waterloo, Ontario, Canada, 2010

© Jeyran Amirloo Abolfathi 2010

I hereby declare that I am the sole author of this thesis. This is a true copy of the thesis, including any required final revisions, as accepted by my examiners.

I understand that my thesis may be made electronically available to the public.

Abstract

This thesis studies quantum coherence in macroscopic and mesoscopic dissipative electrical circuits, including LC circuits, microwave resonators, and Josephson junctions.

For the LC resonator and the terminated transmission line microwave resonator, second quantization is carried out for the lossless system and dissipation is modeled as the coupling to a bath of harmonic oscillators. Stationary states of the linear and nonlinear resonator circuits as well as the associated energy levels are found, and the time evolution of uncertainty relations for the observables such as flux, charge, current, and voltage are obtained. Coherent states of both the lossless and weakly dissipative circuits are studied within a quantum optical approach based on a Fokker-Planck equation for the P-representation of the density matrix which has been utilized to obtain time-variations of the averages and uncertainties of circuit observables.

Macroscopic quantum tunneling is addressed for a driven dissipative Josephson resonator from its metastable current state to the continuum of stable voltage states. The Caldeira-Leggett method and the instanton path integral technique have been used to find the tunneling rate of a driven Josephson junction from a zero-voltage state to the continuum of the voltage states in the presence of dissipation. Upper and lower bounds are obtained for the tunneling rate at the intermediate loss and approximate closed form expressions are derived for the overdamped and underdamped limits.

Acknowledgements

I would like to express my gratitude to my supervisor, Professor A. Hamed Majedi, for his support, encouragement, and guidance.

I would like to thank Professor Anthony J. Leggett for his guidance and illuminating discussions during his summer visits from the institute for quantum computing (IQC).

I am also thankful to my committee members, Professor Hany Aziz and Professor Adrian Lupascu for taking their time to review my thesis.

Last, but not least, I would like to thank my husband for standing by me and believing in me, without his love and support I would never be able to do this work.

To the memory of my father.

Contents

List of Tables	ix
List of Figures	xi
1 Quantization of LC Resonator	1
1.1 Introduction	1
1.2 Classical LC Resonator	2
1.2.1 The Lagrangian Formulation	3
1.2.2 The Hamiltonian Formulation	5
1.3 Quantum LC Resonator	5
1.3.1 Diagonalization of the Hamiltonian	6
1.3.2 Uncertainty Relations	7
1.3.3 Density Matrix Method	12
1.4 Quantum RLC Resonator	16
1.4.1 General Reservoir Theory	16
1.4.2 Field Damping and Fokker-Planck Equation	17
1.4.3 Uncertainty Relations	21
1.5 Summary and Discussion	22

2	Quantization of Microwave Resonator	26
2.1	Introduction	26
2.2	Classical Microwave Resonator	27
2.2.1	The Lagrangian Formulation	30
2.2.2	The Hamiltonian Formulation	31
2.3	Quantum Microwave Resonator	33
2.3.1	Diagonalization of the Hamiltonian	34
2.3.2	Uncertainty Relations	35
2.3.3	Density Matrix	38
2.4	Quantum Damped Microwave Resonator	39
2.4.1	Field Damping and Fokker-Planck Equation	39
2.4.2	Uncertainty Relations	41
2.5	Summary and Discussion	41
3	Josephson Anharmonic Resonator	44
3.1	Introduction	44
3.2	Josephson Tunneling	45
3.3	Classical Dynamics of Josephson Junction	50
3.3.1	The Lagrangian and Hamiltonian of Unbiased Josephson Resonator	55
3.3.2	The Lagrangian and Hamiltonian of Driven Josephson Resonator .	57
3.4	Quantization of Unbiased Josephson Resonator	59
3.5	Quantization of Driven Josephson Resonator	65
3.6	Summary and Discussions	66
4	Macroscopic Tunneling and the Caldeira-Leggett Method	68
4.1	Introduction	68

4.2	Tunneling and Dissipation	70
4.3	The Instanton Technique for Isolated Systems	77
4.4	The Instanton Technique for Damped Systems	78
4.5	Quadratic Plus Cubic Potential	82
4.6	Lagrangian of a Damped LC Resonator	84
4.7	Damped Harmonic Oscillator	86
4.8	The High- and Low-Temperature Limits	89
4.9	Summary and Discussion	90
5	Concluding Remarks	92
	Bibliography	96
	Appendices	101
A	Single Harmonic Oscillator	102
B	Coherent States	105
C	Classical Damping of an RLC Resonator	108
D	Density Matrix of a Harmonic Oscillator	112

List of Tables

- 1.1 Lagrangian formulation for an LC circuit with different choice of the independent variable. 4

List of Figures

1.1	An LC circuit.	3
1.2	Uncertainty for the number states of an LC resonator. Here, $a_1 \equiv (a^\dagger + a)/2$ and $a_2 \equiv i(a^\dagger - a)/2$	10
1.3	Uncertainty for the coherent states of an LC resonator. Here, $a_1 \equiv (a^\dagger + a)/2$ and $a_2 \equiv i(a^\dagger - a)/2$	11
1.4	Time evolution of the P-representation of a lossless LC resonator initially at a coherent state $ \alpha_0\rangle$. Here $L=1\mu\text{H}$, $C=10\text{nF}$, and $\omega_0=10$ Mrad/s. The initial delta function revolves around a circle, centered at the origin of the complex α -plane with a radius $ \alpha_0 $, at an angular frequency of ω_0 without attenuation or broadening.	15
1.5	Time evolution of the P-representation of an RLC resonator initially at a coherent state $ \alpha_0 = 1\rangle$. Here $L=1\mu\text{H}$, $C=10\text{nF}$, $R=100\Omega$, and $\omega_0=10$ Mrad/s. The initial delta function moves on an exponential spiral towards $ 0\rangle$. The P-representation broadens and its amplitude exponentially approaches to the final value $1/\pi\bar{n}_{th}$	20
1.6	The time evolution of $\langle\hat{\Phi}\rangle$ and $\langle\hat{Q}\rangle$ for an RLC resonator with $L=1\mu\text{H}$, $C=10\text{nF}$, $R=100\Omega$, and $\omega_0=10$ Mrad/s.	22
1.7	The time evolution of normalized uncertainty product $2(\Delta\Phi\cdot\Delta Q)/\hbar$ for an RLC resonator with $L=1\mu\text{H}$, $C=10\text{nF}$, $R=100\Omega$, and $\omega_0=10$ Mrad/s.	23
2.1	A microwave resonator (MR) resulted by an open-circuited transmission line (TL).	27

2.2	The circuit model of an infinitesimal length of a lossless TL.	28
3.1	Overlap of the macroscopic wavefunction in a Josephson junction.	47
3.2	RCSJ equivalent circuit model of a biased Josephson junction.	50
3.3	Tilted washboard potential associated with a Josephson junction.	52
3.4	Cubic approximation to the tilted washboard potential of a Josephson junction under small bias around its minimum	53
3.5	RCSJ equivalent circuit model of an unbiased Josephson junction.	55
3.6	Deviation of the eigenenergies from that of an SHO for an unbiased Josephson resonator with $I_c=200\mu A$ and $C = 0.5\text{pF}$	62
3.7	The energy separation between adjacent eigenstates of an unbiased Josephson resonator with $I_c=200\mu A$ and $C = 0.5\text{pF}$	63
3.8	The fidelity to pure number states for the eigenstates of an unbiased Josephson resonator with $I_c=200\mu A$ and $C = 0.5\text{pF}$	64
4.1	The form of the potential $V(q)$ considered in the subsequent calculations.	71
4.2	The lower and upper limits of the change in the exponent of tunneling probability in the case of quadratic plus cubic potential	83
4.3	Circuit Configurations	88
C.1	A parallel RLC circuit.	109
C.2	Classical damping of a parallel RLC resonator with $L=1\mu\text{H}$, $C=10\text{nF}$, and $\omega_0=10\text{ Mrad/s}$. 111	

Chapter 1

Quantization of LC Resonator

1.1 Introduction

To develop a systematic approach for investigation of the quantum mechanical behavior of electric and electronic circuits, the quantization of an LC circuit is the most prominent starting point. LC circuits not only constitute the building block of linear electrical circuits [1], but also comprise an essential part of passive devices, such as resonators, filters, and couplers, as well as active components including parametric amplifiers [2] and oscillators, modulators, and demodulators [3]. Moreover, microwave transmission lines and resonators, which are an important component of superconducting qubits, can be conceived as a network of coupled LC resonators [4]. Therefore, the quantization of LC circuits has direct applications in the evaluation of the performance parameters for many classical and quantum devices. Furthermore, an LC circuit resembles an electrical single harmonic oscillator (SHO) where the electric and magnetic energies oscillate between the capacitor and the inductor through the circuit variables, namely the current, voltage, charge, and flux [5]. Given the significance of the SHO problem in quantum mechanics, the quantiza-

tion of LC circuit enables many of the methods and techniques associated with SHO to be incorporated in the problem of quantum treatment of electrical circuits.

This chapter starts with the development of Lagrangian and Hamiltonian formulations of a classical LC circuit to provide a systematic approach for finding the dynamical conjugate variables. The classical Hamiltonian is then quantized according to the standard quantization recipe. By means of introducing the creation and annihilation operators, the problem is converted to that of an SHO where the uncertainty in the circuit variables are calculated. In the next step, the problem will be formulated in terms of the density matrix method, utilizing the P-representation, which is used to study a damped RLC circuit. The time evolution of the density matrix for an RLC circuit starting from a coherent state is derived and is compared to its classical behavior.

1.2 Classical LC Resonator

The classical dynamics of the LC circuit of Figure 1.1 can be found from the Kirchhoff's voltage and current laws (KVL and KCL)

$$i + C \frac{dv}{dt} = 0, \quad (1.1a)$$

$$v - L \frac{di}{dt} = 0. \quad (1.1b)$$

Equivalently, the capacitor's electric charge Q and the inductor's magnetic flux Φ may be used as the dynamical variables

$$\Phi + L \frac{dQ}{dt} = 0, \quad (1.2a)$$

$$Q - C \frac{d\Phi}{dt} = 0. \quad (1.2b)$$

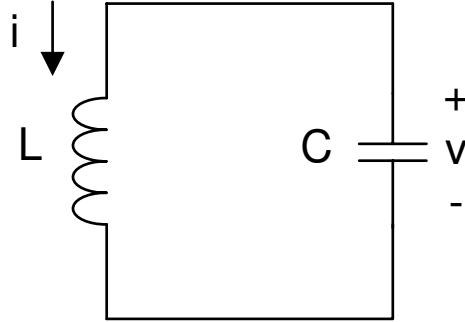


Figure 1.1: An LC circuit.

Equation sets (1.1) and (1.2) comprise the system's equations of motion.

1.2.1 The Lagrangian Formulation

The dynamics of a classical system may be found from the D'Alembert principle. Based on a Lagrangian function \mathcal{L} , the systems's equation(s) of motion are obtained from the Lagrange equation [6, 7]

$$\frac{d}{dt} \left(\frac{\partial \mathcal{L}}{\partial \dot{q}_j} \right) - \frac{\partial \mathcal{L}}{\partial q_j} = 0, \quad (1.3)$$

where q_j are the system's coordinate variables. While the Lagrangian characterizes the system, it is not unique in general. Nevertheless, the Lagrangian of a conservative system may be written as the difference of the kinetic and potential energies. In the lossless circuit of Figure 1.1, the electric and magnetic energies (W_e and W_m) may represent the analogues of the kinetic and potential energies (T and V), respectively. Therefore, the Lagrangian for an LC circuit reads

$$\mathcal{L} = \frac{Q^2}{2C} - \frac{\Phi^2}{2L}. \quad (1.4)$$

\mathcal{L}	q	p	m	ω_0^2	T	V
$\frac{Q^2}{2C} - \frac{\Phi^2}{2L}$	Φ	Q	C	$1/LC$	W_e	W_m
$\frac{\Phi^2}{2L} - \frac{Q^2}{2C}$	Q	$-\Phi$	L	$1/LC$	W_m	W_e
$\frac{1}{2}Cv^2 - \frac{1}{2}Li^2$	i	LCv	L^2C	$1/LC$	W_e	W_m
$\frac{1}{2}Li^2 - \frac{1}{2}Cv^2$	v	$-LCi$	LC^2	$1/LC$	W_m	W_e

Table 1.1: Lagrangian formulation for an LC circuit with different choice of the independent variable.

Here, Φ is taken as the independent variable q whose relation with the dependent variable Q follows from (1.2b). One can readily verify that the equation of motion (1.2a) results from the Lagrange equation (1.3). The canonical momentum p associated with the coordinate variable q is obtained from

$$p = \frac{\partial \mathcal{L}}{\partial \dot{q}_j}. \quad (1.5)$$

Therefore, the problem of an LC circuit corresponds to a simple harmonic oscillator with a Lagrangian

$$\mathcal{L} = \frac{p^2}{2m} - \frac{1}{2}m\omega_0^2q^2, \quad (1.6)$$

with the particle mass

$$m = C, \quad (1.7)$$

and a resonance frequency

$$\omega_0 = \frac{1}{\sqrt{LC}}. \quad (1.8)$$

Obviously, the choice of the independent variable is not unique. Table 1.1 summarizes some of the other options.

1.2.2 The Hamiltonian Formulation

The dynamics of a classical system may be equally formulated through the Hamiltonian function

$$\mathcal{H}(q, p) = \sum_j p_j \dot{q}_j - \mathcal{L}(q, p), \quad (1.9)$$

by means of the Hamilton equations [6]

$$\frac{\partial \mathcal{H}}{\partial p_j} = \dot{q}_j, \quad (1.10a)$$

$$\frac{\partial \mathcal{H}}{\partial q_j} = -\dot{p}_j, \quad (1.10b)$$

where q_j and p_j are the canonical coordinates and momenta, respectively. For conservative forces the Hamiltonian is the total energy of the system, i.e. $T + V$.

According to (1.9), the Hamiltonian for an LC circuit reads

$$\mathcal{H} = \frac{Q^2}{2C} + \frac{\Phi^2}{2L}, \quad (1.11)$$

which corresponds to the Hamiltonian of a single harmonic oscillator

$$\mathcal{H} = \frac{p^2}{2m} + \frac{1}{2}m\omega_0^2 q^2, \quad (1.12)$$

where the mass and resonance frequency are given by (1.7) and (1.8).

1.3 Quantum LC Resonator

The variables q and p representing the dynamics of a classical system may take real values. To study the quantum mechanical dynamics of the system, however, these variables

must be replaced by the operators \hat{q} and \hat{p} . Since operators do not commute in general, appropriate commutation relations must be established among the quantum operators. By replacing the operators for the corresponding classical variables in \mathcal{H} , the system's quantum Hamiltonian operator H is obtained. By means of necessary symmetrization, the Hamiltonian should be cast into a Hermitian form [8]. The time evolution of any operator \hat{O} associated with the system follows the Heisenberg equation of motion

$$\frac{\partial \hat{O}}{\partial t} = \frac{i}{\hbar} [H, \hat{O}], \quad (1.13)$$

where \hbar is the reduced Planck's constant and the commutator of any two operators is defined as

$$[\hat{O}_1, \hat{O}_2] = \hat{O}_1 \hat{O}_2 - \hat{O}_2 \hat{O}_1. \quad (1.14)$$

The Hamiltonian operator H for the LC circuit is, therefore, obtained from the quantization of (1.11)

$$H = \frac{\hat{Q}^2}{2C} + \frac{\hat{\Phi}^2}{2L}, \quad (1.15)$$

with the following commutation relation

$$[\hat{Q}, \hat{\Phi}] = i\hbar. \quad (1.16)$$

1.3.1 Diagonalization of the Hamiltonian

While in the Heisenberg picture, it is more convenient to work with a basis where H is diagonal. The Hamiltonian (1.15) represents that of a single harmonic oscillator

$$H = \frac{\hat{p}^2}{2m} + \frac{1}{2} m \omega_0^2 \hat{q}^2, \quad (1.17)$$

where $m = C$ and $\omega_0^2 = 1/LC$. According to the appendix A, H can be diagonalized by introducing the annihilation and creation operators, which may be explicitly written in terms of $\hat{\Phi}$ and \hat{Q}

$$a = \left(\frac{1}{2\hbar} \sqrt{\frac{C}{L}} \right)^{1/2} \hat{\Phi} + i \left(\frac{1}{2\hbar} \sqrt{\frac{L}{C}} \right)^{1/2} \hat{Q}, \quad (1.18a)$$

and

$$a^\dagger = \left(\frac{1}{2\hbar} \sqrt{\frac{C}{L}} \right)^{1/2} \hat{\Phi} - i \left(\frac{1}{2\hbar} \sqrt{\frac{L}{C}} \right)^{1/2} \hat{Q}. \quad (1.18b)$$

The Hamiltonian in turn reads

$$H = \hbar\omega_0 \left(a^\dagger a + \frac{1}{2} \right). \quad (1.19)$$

According to the appendix A, the circuit operators can be explicitly written in terms of the annihilation and creation operators

$$\hat{\Phi} = \left(\frac{\hbar}{2} \sqrt{\frac{L}{C}} \right)^{1/2} (a^\dagger + a), \quad (1.20a)$$

and

$$\hat{Q} = i \left(\frac{\hbar}{2} \sqrt{\frac{C}{L}} \right)^{1/2} (a^\dagger - a). \quad (1.20b)$$

Any other circuit variable can be quantized to an operator in terms on a and a^\dagger .

1.3.2 Uncertainty Relations

Similar to an SHO, one can find relations governing on the expectation values of the circuit variables of an LC resonator, which are in fact measurable in a laboratory. Referring to the correspondence of the magnetic flux and the electric charge to the position and momentum

operators of an SHO, one can readily find the following for the number states $|n\rangle$

$$\langle \hat{\Phi} \rangle = 0, \quad (1.21a)$$

$$\langle \hat{Q} \rangle = 0, \quad (1.21b)$$

$$(\Delta \hat{\Phi})^2 = \hbar \sqrt{\frac{L}{C}} \left(n + \frac{1}{2} \right), \quad (1.21c)$$

$$(\Delta \hat{Q})^2 = \hbar \sqrt{\frac{C}{L}} \left(n + \frac{1}{2} \right). \quad (1.21d)$$

where for an arbitrary operator \hat{O} ,

$$(\Delta \hat{O})^2 = \langle \hat{O}^2 \rangle - \langle \hat{O} \rangle^2. \quad (1.22)$$

The above relations can be rewritten in terms of the current and voltage operators

$$\langle \hat{i} \rangle = 0, \quad (1.23a)$$

$$\langle \hat{v} \rangle = 0, \quad (1.23b)$$

$$(\Delta \hat{i})^2 = \frac{\hbar \omega_0}{L} \left(n + \frac{1}{2} \right), \quad (1.23c)$$

$$(\Delta \hat{v})^2 = \frac{\hbar \omega_0}{C} \left(n + \frac{1}{2} \right). \quad (1.23d)$$

The first two relations in both sets show that the average of the current, voltage, flux, and charge vanish. This point simply means that these circuit variables do not have a dc component, which is consistent with the sinusoidal form of the solutions of a classical LC resonator. The last two relations, however, show that the uncertainty in the voltage

and flux (current and charge) may be reduced by using a larger capacitor (inductor) and a smaller inductor (capacitor) while maintaining their product, i.e. the resonance frequency, constant. Nevertheless, reducing the uncertainty of a variable, by this method, is at the price of increasing the uncertainty of its conjugate variable. The uncertainty product, in general, is a quantum mechanical fundamental limit

$$\Delta\hat{\Phi} \cdot \Delta\hat{Q} = \hbar \left(n + \frac{1}{2} \right), \quad (1.24a)$$

and

$$\Delta\hat{v} \cdot \Delta\hat{i} = \hbar\omega_0^2 \left(n + \frac{1}{2} \right). \quad (1.24b)$$

According to the Heisenberg uncertainty principle

$$\Delta\hat{q} \cdot \Delta\hat{p} \geq \frac{\hbar}{2}, \quad (1.25)$$

the vacuum state $|0\rangle$ is a minimum-uncertainty state. Figure 1.2 illustrates the uncertainty and averages of the number states.

In practice, the actual state of an LC resonator can be best related to coherent states $|\alpha\rangle$,

$$|\alpha\rangle = e^{-\frac{1}{2}|\alpha|^2} \sum_{n=0}^{\infty} \frac{\alpha^n}{\sqrt{n!}} |n\rangle. \quad (1.26)$$

According to the appendix B where the properties of the coherent states are reviewed, the average and uncertainty of the circuit variables for $|\alpha\rangle$ follow

$$\langle\hat{\Phi}\rangle = \left(\frac{\hbar}{2} \sqrt{\frac{L}{C}} \right)^{\frac{1}{2}} (\alpha + \alpha^*) = \left(2\hbar \sqrt{\frac{L}{C}} \right)^{\frac{1}{2}} \Re e(\alpha), \quad (1.27a)$$

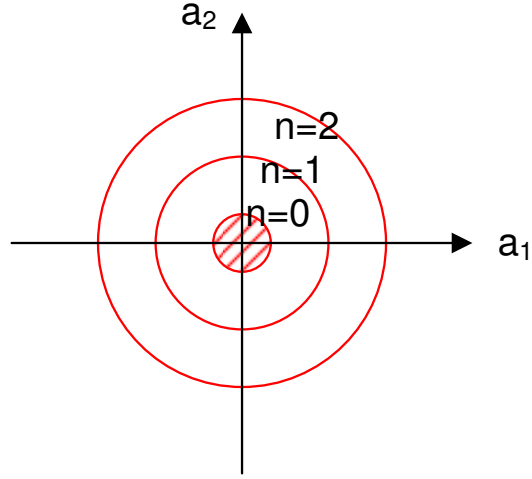


Figure 1.2: Uncertainty for the number states of an LC resonator. Here, $a_1 \equiv (a^\dagger + a)/2$ and $a_2 \equiv i(a^\dagger - a)/2$.

$$\langle \hat{Q} \rangle = i \left(\frac{\hbar}{2} \sqrt{\frac{C}{L}} \right)^{\frac{1}{2}} (\alpha^* - \alpha) = \left(2\hbar \sqrt{\frac{C}{L}} \right)^{\frac{1}{2}} \Im m(\alpha), \quad (1.27b)$$

$$(\Delta \hat{\Phi})^2 = \frac{\hbar}{2} \sqrt{\frac{L}{C}}, \quad (1.27c)$$

$$(\Delta \hat{Q})^2 = \frac{\hbar}{2} \sqrt{\frac{C}{L}}. \quad (1.27d)$$

The above relations can be rewritten in terms of the current and voltage operators

$$\langle \hat{i} \rangle = \left(\frac{2\hbar\omega_0}{L} \right)^{\frac{1}{2}} \Re e(\alpha), \quad (1.28a)$$

$$\langle \hat{v} \rangle = \left(\frac{2\hbar\omega_0}{C} \right)^{\frac{1}{2}} \Im m(\alpha), \quad (1.28b)$$

$$(\Delta \hat{i})^2 = \frac{\hbar\omega_0}{2L}, \quad (1.28c)$$

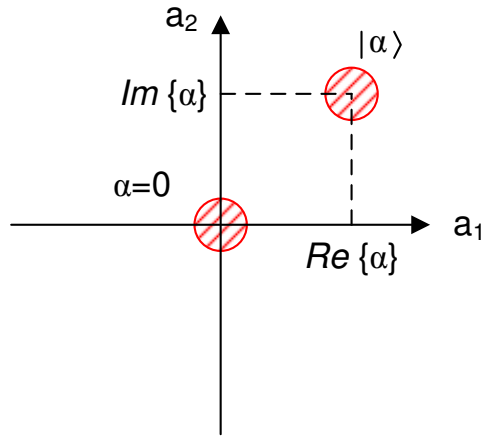


Figure 1.3: Uncertainty for the coherent states of an LC resonator. Here, $a_1 \equiv (a^\dagger + a)/2$ and $a_2 \equiv i(a^\dagger - a)/2$.

$$(\Delta \hat{v})^2 = \frac{\hbar \omega_0}{2C}. \quad (1.28d)$$

The uncertainty products in turn follow

$$\Delta \hat{\Phi} \cdot \Delta \hat{Q} = \frac{\hbar}{2}, \quad (1.29a)$$

and

$$\Delta \hat{v} \cdot \Delta \hat{i} = \frac{\hbar \omega_0^2}{2}. \quad (1.29b)$$

Therefore, the coherent states $|\alpha\rangle$ are minimum-uncertainty states, as is illustrated by Figure 1.3.

1.3.3 Density Matrix Method

The dynamics of a quantum system can be fully represented through its density operator

$$\hat{\rho} = \sum_{\psi} P_{\psi} |\psi\rangle\langle\psi|, \quad (1.30)$$

where $|\psi\rangle$ is any possible state of the system and P_{ψ} is the probability of the system being found in the state $|\psi\rangle$ [9]. The expectation value of any field operator \hat{O} is then given by

$$\langle\hat{O}\rangle = \text{Tr}\{\hat{O}\hat{\rho}\}, \quad (1.31)$$

where Tr stands for trace. According to (1.13), the equation of motion for the density operator of an LC resonator reads

$$\dot{\hat{\rho}} = i\omega_0(a^\dagger a \hat{\rho} - \hat{\rho} a^\dagger a). \quad (1.32)$$

Here, the density operator is expanded in terms of the coherent states $|\alpha\rangle$, i.e. the P-representation,

$$\hat{\rho} = \int P(\alpha, \alpha^*, t) |\alpha\rangle\langle\alpha| d^2\alpha. \quad (1.33)$$

Based on the properties of the coherent states, which are reviewed in the appendix B,

$$(a^\dagger a |\alpha\rangle\langle\alpha| - |\alpha\rangle\langle\alpha| a^\dagger a) = \left(\alpha \frac{\partial}{\partial\alpha} - \alpha^* \frac{\partial}{\partial\alpha^*}\right) |\alpha\rangle\langle\alpha|. \quad (1.34)$$

Substituting (1.34) in (1.32),

$$\int d^2\alpha \dot{P}(\alpha, \alpha^*, t) |\alpha\rangle\langle\alpha| = i\omega_0 \int d^2\alpha P(\alpha, \alpha^*, t) \left[\alpha \frac{\partial}{\partial\alpha} - \alpha^* \frac{\partial}{\partial\alpha^*}\right] |\alpha\rangle\langle\alpha|. \quad (1.35)$$

Integrating by part, the right hand side of (1.35) reads

$$i\omega_0 \{(\alpha - \alpha^*)P(\alpha, \alpha^*, t)|\alpha\rangle\langle\alpha|\} \Big|_{-\infty}^{+\infty} - \int (\alpha \frac{\partial}{\partial \alpha} - \alpha^* \frac{\partial}{\partial \alpha^*})P(\alpha, \alpha^*, t)|\alpha\rangle\langle\alpha|. \quad (1.36)$$

Thus,

$$\dot{P}(\alpha, \alpha^*, t) = -i\omega_0(\alpha \frac{\partial}{\partial \alpha} - \alpha^* \frac{\partial}{\partial \alpha^*})P. \quad (1.37)$$

If the circuit is initially at a coherent state $|\alpha_0\rangle$, then

$$P(\alpha, \alpha^*, 0) = \delta^2(\alpha - \alpha_0) = \lim_{\epsilon \rightarrow 0} \frac{1}{\pi\epsilon} \exp\left(\frac{-|\alpha - \alpha_0|^2}{\epsilon}\right). \quad (1.38)$$

Taking P in the form of a general Gaussian distribution

$$P(\alpha, \alpha^*, t) = \exp[-a(t) + b(t)\alpha + c(t)\alpha^* - d(t)\alpha\alpha^*], \quad (1.39)$$

the initial conditions follow [9]

$$a(0) = \frac{|\alpha_0|^2}{\epsilon} + \ln(\pi\epsilon), \quad (1.40a)$$

$$b(0) = \frac{\alpha^*}{\epsilon}, \quad (1.40b)$$

$$c(0) = \frac{\alpha}{\epsilon}, \quad (1.40c)$$

$$d(0) = \frac{1}{\epsilon}. \quad (1.40d)$$

Substituting the form (1.39) into (1.37),

$$(-\dot{a} + \dot{b} + \dot{c}\alpha^* - \dot{d}\alpha\alpha^*)P = -i\omega_0(b\alpha - c\alpha^*)P. \quad (1.41)$$

Hence,

$$\begin{aligned} \dot{a} &= 0 & a(t) &= a_0, \\ \dot{b} &= -i\omega_0 b & \Rightarrow & b(t) = b_0 e^{-i\omega_0 t}, \\ \dot{c} &= +i\omega_0 c & c(t) &= c_0 e^{+i\omega_0 t}, \\ \dot{d} &= 0 & d(t) &= 0, \end{aligned}$$

and

$$P(\alpha, \alpha^*, t) = \delta^2(\alpha - \alpha_0 e^{+i\omega_0 t}), \quad (1.42)$$

which means

$$|\psi(t)\rangle = |\alpha_0 e^{i\omega_0 t}\rangle. \quad (1.43)$$

Figure 1.4 illustrates this point, where the P-representation of the initial coherent state $|\alpha_0\rangle$, i.e. $\delta^2(\alpha - \alpha_0)$, revolves around a circle in time without attenuation or broadening.

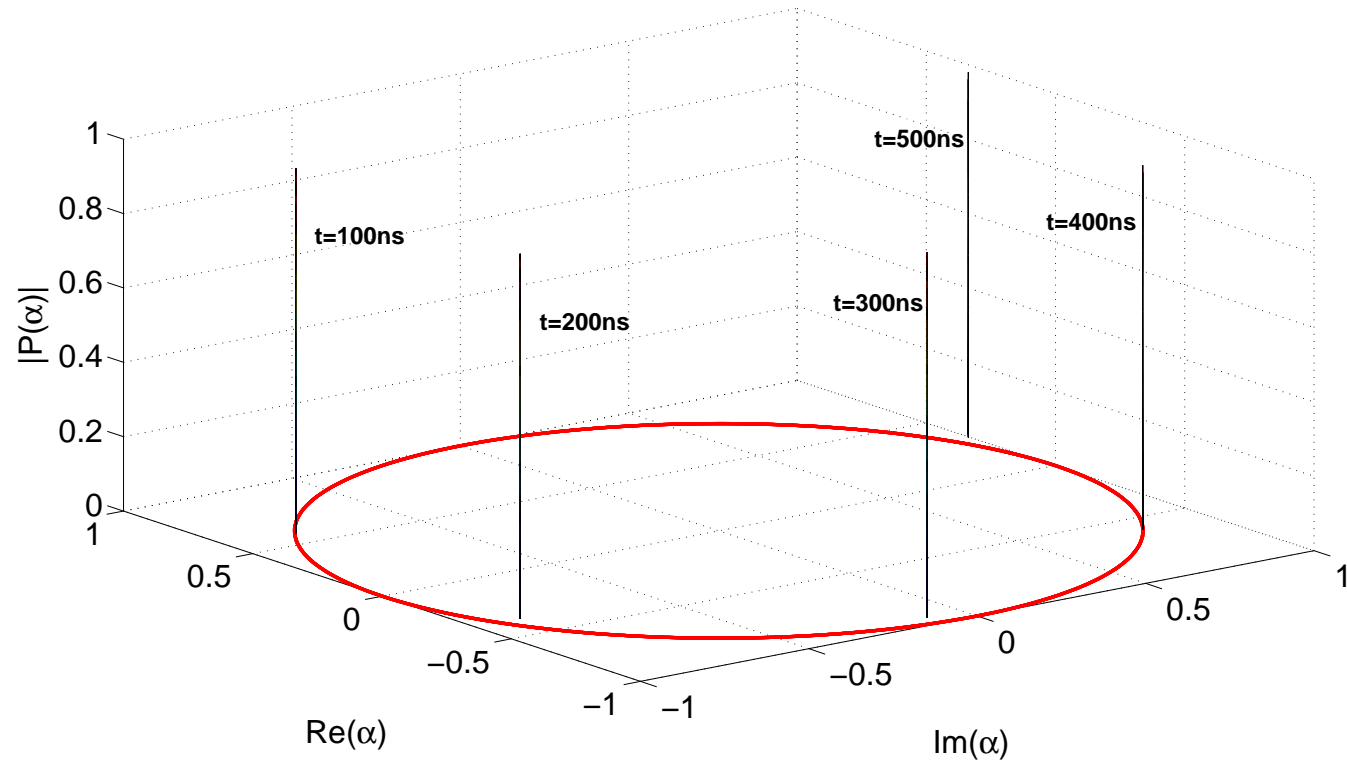


Figure 1.4: Time evolution of the P-representation of a lossless LC resonator initially at a coherent state $|\alpha_0\rangle$. Here $L=1\mu\text{H}$, $C=10\text{nF}$, and $\omega_0=10\text{ Mrad/s}$. The initial delta function revolves around a circle, centered at the origin of the complex α -plane with a radius $|\alpha_0|$, at an angular frequency of ω_0 without attenuation or broadening.

1.4 Quantum RLC Resonator

The dissipation in the LC resonator circuit is usually modeled by a linear resistance R . The effect of the resistor R is equivalent to coupling the LC resonator to a bath of Harmonic oscillators. The resulting Hamiltonian then reads [9]

$$\mathcal{V} = \hbar \sum_k g_k [b_k^\dagger a e^{-i(\omega_0 - \omega_k)t} + a^\dagger b_k e^{i(\omega_0 - \omega_k)t}], \quad (1.44)$$

where ω_0 is the resonance frequency of the LC circuit, ω_k and g_k respectively are the eigenfrequency and the coupling factor of the mode \mathbf{k} in the reservoir, and b_k^\dagger and b_k are the corresponding creation and annihilation operators of the reservoir modes.

1.4.1 General Reservoir Theory

For a system S interacting with a reservoir R the joint density matrix $\hat{\rho}_{SR}$ follows

$$i\hbar \dot{\hat{\rho}}_{SR} = [\mathcal{V}, \hat{\rho}_{SR}], \quad (1.45)$$

where \mathcal{V} is the interaction Hamiltonian. The system's density matrix is simply

$$\hat{\rho}_S = Tr_R\{\hat{\rho}_{SR}\}. \quad (1.46)$$

If the dissipation is small, i.e. the interaction between the system and the reservoir is weak, the joint density matrix may be written as [9]

$$\hat{\rho}_{SR} = \hat{\rho}_S \otimes \hat{\rho}_R + \hat{\rho}_c, \quad (1.47)$$

where $\hat{\rho}_c$ is of higher order in \mathcal{V} . Clearly,

$$Tr_R\{\hat{\rho}_c\} = 0. \quad (1.48)$$

Moreover, if it is assumed that $\dot{\hat{\rho}}_S(t)$ only depends on $\hat{\rho}_S(t)$, i.e. the system is memoryless or more formally the process is Markovian, the time evolution of the system's density matrix obeys the following master equation

$$\dot{\hat{\rho}}_S = -\frac{i}{\hbar}Tr_R[\mathcal{V}(t), \hat{\rho}_S(t_i) \otimes \hat{\rho}_R(t_i)] - \frac{1}{\hbar^2}Tr_R \int_{t_i}^t [\mathcal{V}(t), [\mathcal{V}(t'), \hat{\rho}_S(t) \otimes \hat{\rho}_R(t_i)]]dt'. \quad (1.49)$$

1.4.2 Field Damping and Fokker-Planck Equation

Assuming that the reservoir is at thermal equilibrium, i.e. a thermal bath, the equation of motion for the density matrix of the LC circuit reads

$$\begin{aligned} \dot{\hat{\rho}} = & -\frac{\eta}{2}\bar{n}_{th}(aa^\dagger\hat{\rho} - 2a^\dagger\hat{\rho}a + \hat{\rho}a^\dagger a) \\ & -\frac{\eta}{2}(\bar{n}_{th} + 1)(a^\dagger a\hat{\rho} - 2a\hat{\rho}a^\dagger + \hat{\rho}aa^\dagger), \end{aligned} \quad (1.50)$$

where η is related to the resonator quality factor Q through $\eta = \omega_0/Q$ and

$$\bar{n}_{th} = \frac{1}{\exp\left(\frac{\hbar\omega_0}{k_B T} - 1\right)} \quad (1.51)$$

is the mean number of quanta at ω_0 in the reservoir and k_B is the Boltzmann constant¹.

At zero temperature, where $\bar{n}_{th} = 0$, (1.50) reduces to

$$\dot{\rho} = -\frac{\eta}{2}(a^\dagger a \hat{\rho} - 2a \hat{\rho} a^\dagger + \hat{\rho} a^\dagger a). \quad (1.52)$$

Using the P-representation (2.39),

$$\dot{P} = \frac{\eta}{2} \left(\frac{\partial}{\partial \alpha} \alpha + \frac{\partial}{\partial \alpha^*} \alpha^* \right) P + \eta \bar{n}_{th} \frac{\partial^2 P}{\partial \alpha \partial \alpha^*}, \quad (1.53)$$

which is the Fokker-Plank equation for the P-representation. If we assume that the LC resonator is initially at a coherent state $|\alpha_0\rangle$, then

$$P(\alpha, \alpha_0, 0) = \delta^2(\alpha - \alpha_0). \quad (1.54)$$

Given that the P-distribution is Gaussian at thermal equilibrium, we substitute the ansatz of (1.39), along with the initial conditions (1.40), into (1.53) [9]. Therefore,

$$\dot{d} = \eta(d - \bar{n}_{th}d^2), \quad (1.55a)$$

$$\dot{c} = \eta\left(\frac{c}{2} - \bar{n}_{th}cd\right), \quad (1.55b)$$

$$\dot{b} = \eta\left(\frac{b}{2} - bd\right), \quad (1.55c)$$

$$\dot{a} = \eta(1 + \bar{n}_{th}(bc - d)), \quad (1.55d)$$

¹Derivation of \bar{n}_{th} is presented in the appendix D

whose solutions are

$$d(t) = \frac{1}{\bar{n}_{th}(1 - e^{-\eta t}) + \epsilon e^{-\eta t}}, \quad (1.56a)$$

$$c(t) = \frac{\alpha_0 e^{-\eta t}}{\bar{n}_{th}(1 - e^{-\eta t}) + \epsilon e^{-\eta t}}, \quad (1.56b)$$

$$b(t) = \frac{\alpha_0^*}{\bar{n}_{th}(1 - e^{-\eta t}) + \epsilon e^{-\eta t}}, \quad (1.56c)$$

$$a(t) = \frac{|\alpha_0|^2 e^{-\eta t}}{\bar{n}_{th}(1 - e^{-\eta t}) + \epsilon e^{-\eta t}} + \ln \left\{ \pi \left[\bar{n}_{th}(1 - e^{-\eta t}) + \epsilon e^{-\eta t} \right] \right\}. \quad (1.56d)$$

Replacing the solutions into the Gaussian form (1.39), the time evolution of the P-representation follows

$$P(\alpha, \alpha^*, t) = \frac{1}{\pi D(t)} \exp \left[-\frac{|\alpha - \alpha_0 U(t)|^2}{D(t)} \right], \quad (1.57)$$

where

$$D(t) = \bar{n}_{th}(1 - e^{-\eta t}), \quad (1.58)$$

and

$$U(t) = e^{-\frac{\eta t}{2}} e^{-i\omega_0 t}. \quad (1.59)$$

Unlike a lossless LC resonator, an RLC resonator initially at a coherent state $|\alpha_0\rangle$ moves towards $|\alpha = 0\rangle$ on an exponential spiral as illustrated by Figure 1.5. This behavior corresponds to the classical relaxation of an RLC resonator as reviewed in the appendix C. While the center of the P-representation follows the spiral, its amplitude decays and its P-representation broadens over the time. The dispersion function $D(t)$ starts from zero, corresponding to a delta function associated with the initial state $|\alpha_0\rangle$, and approaches to its final value \bar{n}_{th} . This point clearly shows that dissipation is always accompanied with dispersion. Therefore, the oscillator transfers its energy to the heat bath and acquires noise.

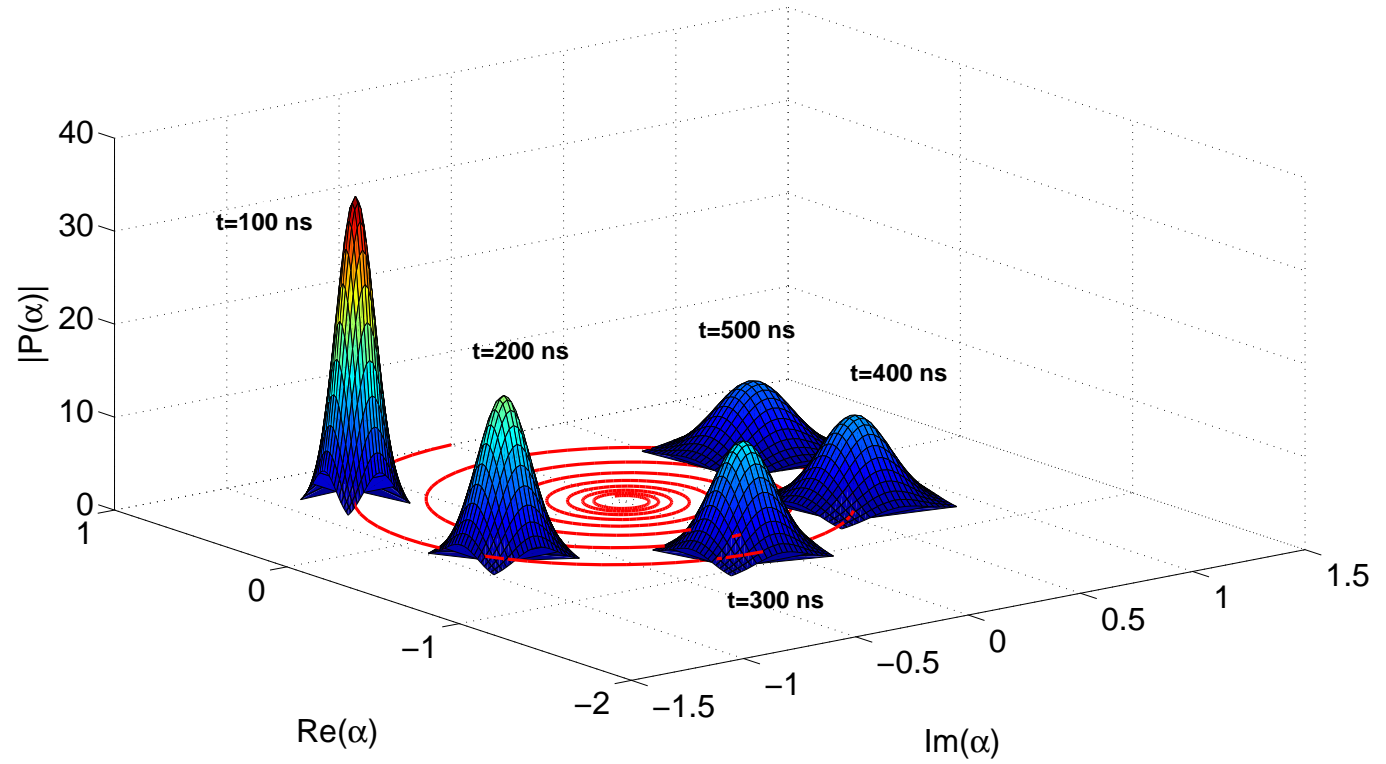


Figure 1.5: Time evolution of the P-representation of an RLC resonator initially at a coherent state $|\alpha_0 = 1\rangle$. Here $L=1\mu\text{H}$, $C=10\text{nF}$, $R=100\Omega$, and $\omega_0=10$ Mrad/s. The initial delta function moves on an exponential spiral towards $|0\rangle$. The P-representation broadens and its amplitude exponentially approaches to the final value $1/\pi\bar{n}_{th}$.

1.4.3 Uncertainty Relations

Once the density operator of a damped oscillator is obtained, it can be used to evaluate the averages and uncertainties of the circuit variables through (1.31). It is straightforward to show that starting from a coherent state $|\alpha\rangle$,

$$\langle \hat{\Phi} \rangle = \left(2\hbar \sqrt{\frac{L}{C}} \right)^{\frac{1}{2}} [|\alpha| e^{-\eta t/2} \cos(\omega_0 t - \phi)], \quad (1.60a)$$

and

$$\langle \hat{Q} \rangle = \left(2\hbar \sqrt{\frac{C}{L}} \right)^{\frac{1}{2}} [-|\alpha| e^{-\eta t/2} \sin(\omega_0 t - \phi)], \quad (1.60b)$$

where $\alpha = |\alpha| e^{i\phi}$ and $\eta = 1/RC$. These relations correspond to an under-damped classical oscillator, as discussed in the appendix C, and are consistent with the assumption of small dissipation. Figure 1.6 depicts the above relations. Moreover,

$$(\Delta \hat{\Phi})^2 = \frac{\hbar}{2} \sqrt{\frac{L}{C}} [1 + 2D(t)], \quad (1.61a)$$

and

$$(\Delta \hat{Q})^2 = \frac{\hbar}{2} \sqrt{\frac{C}{L}} [1 + 2D(t)]. \quad (1.61b)$$

According to (1.23) and $D(0) = 0$, it is clear that the uncertainties of the conjugate variables start from that of a lossless resonator and increases in time, as illustrated in Figure 1.7.

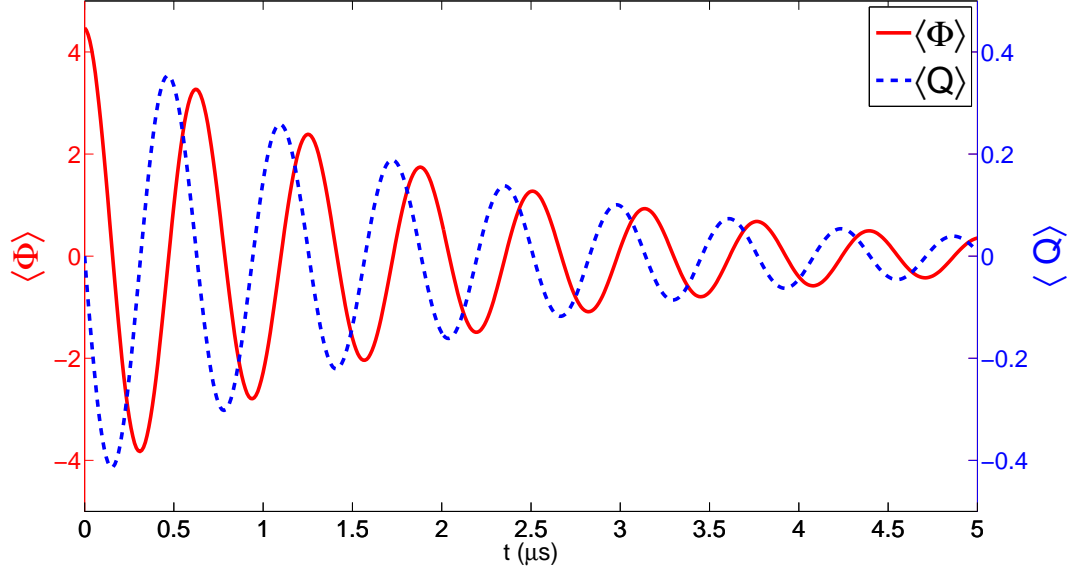


Figure 1.6: The time evolution of $\langle \hat{\Phi} \rangle$ and $\langle \hat{Q} \rangle$ for an RLC resonator with $L=1\mu\text{H}$, $C=10\text{nF}$, $R=100\Omega$, and $\omega_0=10\text{ Mrad/s}$.

1.5 Summary and Discussion

This chapter studied the quantization of an LC resonator. The classical Lagrangian and Hamiltonian of the system were developed by making a correspondence between the magnetic and electric energies to the potential and kinetic energies, respectively. The standard recipe of quantization was in turn applied to the classical Hamiltonian function for constructing the quantum Hamiltonian operator. It turned out that the magnetic flux $\hat{\Phi}$ and electric charge \hat{Q} operators respectively resemble the coordinate and momentum operators \hat{q} and \hat{p} . The resulting Hamiltonian represented a single harmonic oscillator (SHO) with a mass of C and a resonance frequency $\omega_0 = 1/\sqrt{LC}$. By means of the creation and annihilation operators, a^\dagger and a , the Hamiltonian operator was diagonalized. According to the uncertainty relations of an SHO, the averages and uncertainties for the flux, charge,

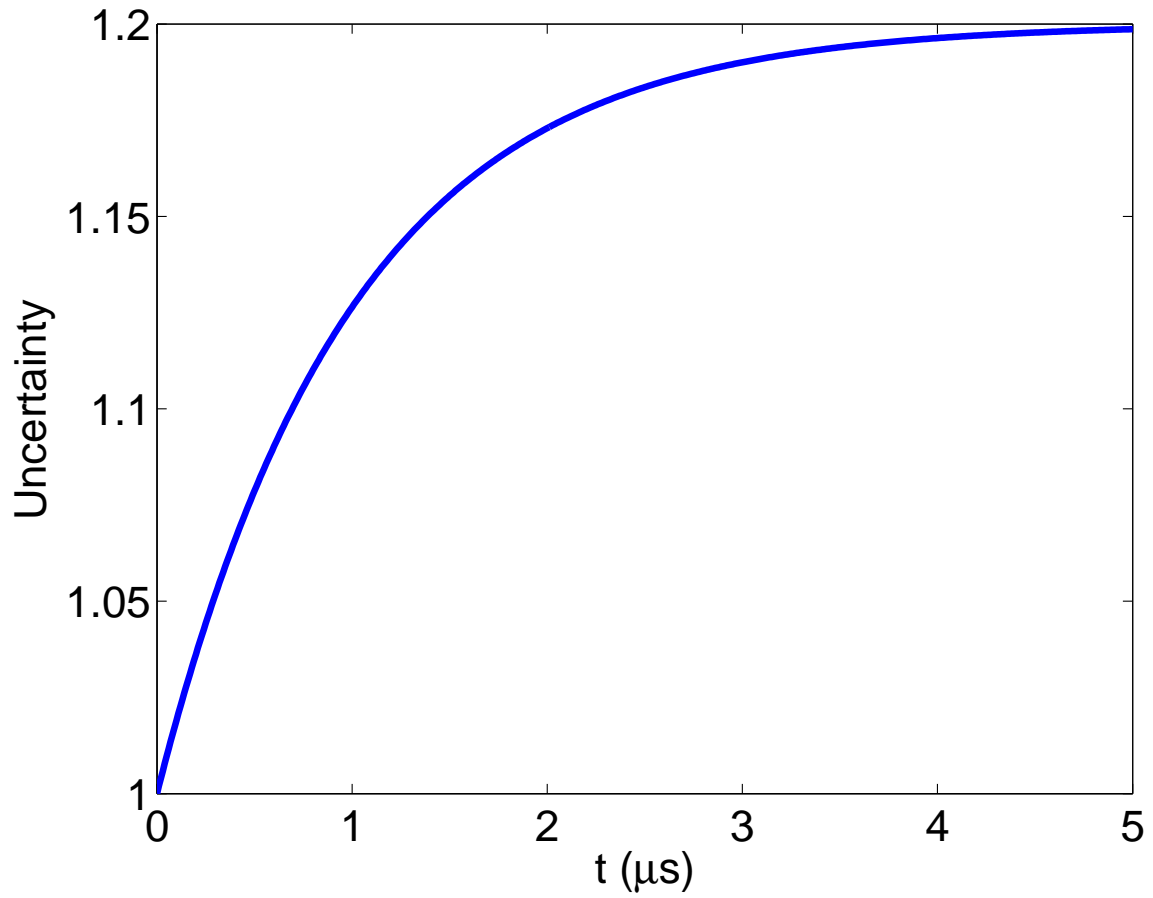


Figure 1.7: The time evolution of normalized uncertainty product $2(\Delta\Phi \cdot \Delta Q)/\hbar$ for an RLC resonator with $L=1\mu\text{H}$, $C=10\text{nF}$, $R=100\Omega$, and $\omega_0=10\text{ Mrad/s}$.

voltage, and current operators were obtained for the number $|n\rangle$ and coherent states $|\alpha\rangle$. Through the time evolution of the LC resonator's density operator, it was shown that a lossless resonator initially at a coherent state $|\alpha_0\rangle$ undergoes only a phase change over the time $|e^{i\omega_0 t}\alpha_0\rangle$. For the analysis of a dissipative resonator, i.e. an RLC circuit, the presence of the dissipative element was modeled as the coupling of the LC oscillator to a bath of SHOs. Assuming small dissipation, i.e. weak coupling to the thermal reservoir, a master equation was derived for the time evolution of the density operator based on a quantum optical approach. It was shown that the P-representation of the density matrix follows the Fokker-Planck equation. Therefore, an RLC resonator initially at a coherent state $|\alpha_0\rangle$ asymptotically approaches to the vacuum state $|0\rangle$. While the P-representation at $t = 0$ corresponds to a delta function at $\alpha = \alpha_0$, the P-representation, at later times, will correspond to Gaussian distributions which constantly broadens and whose center moves on an exponential spiral towards the vacuum state. This point was further illustrated by showing that the averages of the conjugate variables relax to zero according to an under-damped classical resonator. The time evolution of the uncertainties showed that although the resonator starts from a minimum-uncertainty state, the uncertainties increase monotonically over the time and asymptotically approach to their final value. Thus, the dissipative resonator loses its energy to the thermal bath and acquires noise.

In general, for observing the quantum effects the quantum energy of oscillations must be much greater than thermal fluctuations [10]

$$\hbar\omega_0 \gg k_B T. \tag{1.62}$$

For a resonator with $\omega_0=(2\pi)1\text{GHz}$, the temperature should be well below 40mK. Moreover, the quality factor of the resonator must be very high; otherwise the resonator will quickly damps out. Despite the satisfaction of the above requirements, showing that the resonator

behaves quantum mechanically is not straightforward. The transitions between adjacent levels involve quanta of frequency ω_0 which is exactly the frequency of classical oscillations [10]. In fact, an SHO is precisely at the quantum-classical correspondence limit for all quantum numbers [11]. Observation of the zero-point motion of the ground state may be the only direct signature of quantum behavior which is an extremely difficult experiment and requires quantum-limited amplifiers [10].

Alternatively, one can break the correspondence limit by introducing a little anharmonicity into the problem by means of a nonlinear element. An anharmonic potential results in nonuniform separation between the adjacent level. A prominent example of such a circuit is a Josephson junction which is the subject of following chapters. The presence of the Josephson junction enables the observation of the tunneling of a macroscopic variable, which is absolutely quantum mechanical.

Chapter 2

Quantization of Microwave Resonator

2.1 Introduction

The previous chapter studied the quantization of LC resonators as a fundamental element for understanding the quantum mechanical behavior of electrical circuits. Nevertheless, high-frequency electromagnetic resonators are not in the form of lumped-element LC circuits, but rather are realized as microwave cavities [4]. A simple way to realize a microwave resonator (MR) is to terminate a finite length of a microwave transmission line (TL) at both ends. Figure 2.1 illustrates a TL which is open-circuited at both sides. A specific termination would determine the boundary conditions for the current and voltage standing-waves at the loads.

In this chapter, we begin with a brief review of a classical lossless MR. It will be shown that different modes of the cavity can be thought of as independent SHOs. Each of the modes will then be quantized by means of a technique similar to what used for LC resonators in the previous chapter. The dynamics of the system as well as the uncertainty relations will be investigated for a lossless MR, and the discussion of the effects of small

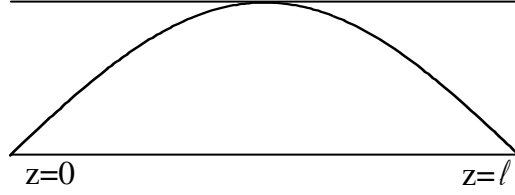


Figure 2.1: A microwave resonator (MR) resulted by an open-circuited transmission line (TL).

dissipation on the decoherence of the eigenstates and evolution of uncertainty parameters will conclude the chapter.

2.2 Classical Microwave Resonator

Within a microwave TL, voltage and current are associated with the transverse component of the electric and magnetic fields propagating along the structure [12]. Therefore, voltage and current must be treated as waves oscillating over the time and space. Figure 2.2 shows the circuit equivalent of an infinitesimal length, dz , of a lossless TL. $L(H/m)$ and $C(F/m)$ are the differential inductance and capacitance of the line, respectively. Thus, the inductance and capacitance of the length dz are Ldz and Cdz . Applying *KVL* and *KCL*,

$$v(z) - v(z + dz) = (Ldz) \frac{\partial i(z)}{\partial t}, \quad (2.1a)$$

and

$$i(z) - i(z + dz) = (Cdz) \frac{\partial v(z + dz)}{\partial t}. \quad (2.1b)$$

Let $dz \rightarrow 0$, therefore

$$\frac{\partial v}{\partial z} = -L \frac{\partial i}{\partial t}, \quad (2.2a)$$

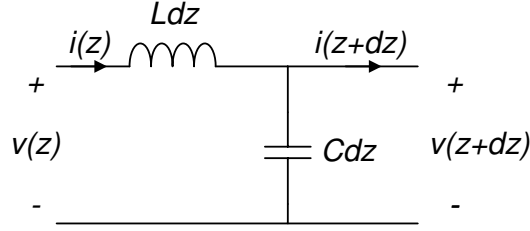


Figure 2.2: The circuit model of an infinitesimal length of a lossless TL.

and

$$\frac{\partial i}{\partial z} = -C \frac{\partial v}{\partial t}. \quad (2.2b)$$

Relations (2.2) are the equations of motion of the system, and yield the so called telegrapher equations

$$\frac{\partial^2 v}{\partial z^2} = \frac{1}{u_p^2} \frac{\partial^2 v}{\partial t^2}, \quad (2.3a)$$

and

$$\frac{\partial^2 i}{\partial z^2} = \frac{1}{u_p^2} \frac{\partial^2 i}{\partial t^2}, \quad (2.3b)$$

where the phase velocity u_p is defined as

$$u_p \equiv \frac{1}{\sqrt{LC}}. \quad (2.4)$$

When a TL is terminated at both ends, with the loads Z_{L1} and Z_{L2} to realize an MR, the voltage and current standing-waves are created. Suppose that the associated reflection coefficients respectively are Γ_1 and Γ_2 , where

$$\Gamma = \frac{Z_L - Z_0}{Z_L + Z_0}, \quad (2.5)$$

and Z_0 is the characteristic impedance of the TL

$$Z_0 = \sqrt{L/C}. \quad (2.6)$$

A reflection coefficient whose magnitude is less than unity, i.e. $|\Gamma| < 1$, indicates transmission of electromagnetic energy to the load. Therefore, to realize a lossless resonator the terminations must yield

$$\Gamma_{1,2} = e^{i\theta_{1,2}}, \quad (2.7)$$

otherwise the MR system will lose energy due to the coupling to the absorbing loads, even though the TL is intrinsically lossless. Since the length of the resonator is finite, the voltage and current waves may be written as Fourier series

$$v(z, t) = \sqrt{\frac{2}{\ell}} \sum_{n=1}^{\infty} V_n(t) \cos(k_n z + \theta_0), \quad (2.8a)$$

and

$$i(z, t) = \sqrt{\frac{2}{\ell}} \sum_{n=1}^{\infty} I_n(t) \sin(k_n z + \theta_0), \quad (2.8b)$$

where ¹

$$\theta_0 = \frac{\theta_1}{2}, \quad (2.9a)$$

and

$$k_n = \frac{2\pi n}{\ell} - \frac{\theta_2 + \theta_1}{2\ell}, \quad (2.9b)$$

¹Clearly, if both ends are open-circuited then $\theta_0 = 0$, and if short-circuited then $\theta_0 = \frac{\pi}{2}$.

and the Fourier amplitudes follow

$$V_n(t) = \sqrt{\frac{2}{\ell}} \int_0^\ell v(z, t) \cos(k_n z + \theta_0) dz, \quad (2.10a)$$

and

$$I_n(t) = \sqrt{\frac{2}{\ell}} \int_0^\ell i(z, t) \sin(k_n z + \theta_0) dz. \quad (2.10b)$$

2.2.1 The Lagrangian Formulation

The magnetic flux density Φ , threading the cross section of the TL at a point z , can be defined through the Faraday's law

$$v = \frac{\partial \Phi}{\partial t}, \quad (2.11a)$$

and according to the circuit model of Fig. 2.2

$$\frac{\partial \Phi}{\partial z} = -Li. \quad (2.11b)$$

Through the introduction of Φ equation (2.2a) is identically satisfied, and the system's equation of motion reduces to

$$\frac{\partial^2 \Phi}{\partial z^2} = \frac{1}{u_p^2} \frac{\partial^2 \Phi}{\partial t^2}. \quad (2.12)$$

The Lagrangian at a point z can be written as the difference between the electric and magnetic energies

$$\mathcal{L}_z = \frac{1}{2} C \left(\frac{\partial \Phi}{\partial t} \right)^2 - \frac{1}{2L} \left(\frac{\partial \Phi}{\partial z} \right)^2. \quad (2.13)$$

It is straightforward to show that the following variational equation yields the equation of motion (2.12),

$$\frac{\partial \mathcal{L}_z}{\partial \Phi} - \frac{\partial}{\partial t} \left[\frac{\partial \mathcal{L}_z}{\partial \left(\frac{\partial \Phi}{\partial t} \right)} \right] - \frac{\partial}{\partial z} \left[\frac{\partial \mathcal{L}_z}{\partial \left(\frac{\partial \Phi}{\partial z} \right)} \right] = 0. \quad (2.14)$$

Taking the flux density as the coordinate variable

$$q = \Phi, \quad (2.15)$$

the canonical momentum is obtained from the Lagrangian

$$p \equiv \frac{\partial \mathcal{L}_z}{\partial \left(\frac{\partial \Phi}{\partial t} \right)} = C \frac{\partial \Phi}{\partial t} = Q, \quad (2.16)$$

where Q is the charge density at the point z along the TL. Finally, the total Lagrangian of the system is

$$\mathcal{L} = \int_0^\ell \mathcal{L}_z dz. \quad (2.17)$$

2.2.2 The Hamiltonian Formulation

The Hamiltonian at a point z along the TL can be found from \mathcal{L}_z ,

$$\mathcal{H}_z \equiv p\dot{q} - \mathcal{L}_z = \frac{1}{2}C \left(\frac{\partial \Phi}{\partial t} \right)^2 + \frac{1}{2L} \left(\frac{\partial \Phi}{\partial z} \right)^2 \quad (2.18a)$$

$$= \frac{Q^2}{2C} + \frac{1}{2L} \left(\frac{\partial \Phi}{\partial z} \right)^2. \quad (2.18b)$$

The total Hamiltonian of the system is then

$$\mathcal{H} = \int_0^\ell \mathcal{H}_z dz. \quad (2.19)$$

Rewriting Φ and Q as Fourier series

$$\Phi(z, t) = \sqrt{\frac{2}{\ell}} \sum_{n=1}^{\infty} \Phi_n(t) \sin(k_n z + \theta_0), \quad (2.20a)$$

and

$$Q(z, t) = \sqrt{\frac{2}{\ell}} \sum_{n=1}^{\infty} Q_n(t) \cos(k_n z + \theta_0), \quad (2.20b)$$

and using the orthogonality of the cosine functions the Hamiltonian reads

$$\mathcal{H} = \sum_{n=1}^{\infty} \left[\frac{Q_n^2}{2C} + k_n^2 \frac{\Phi_n^2}{2L} \right], \quad (2.21)$$

which is the Hamiltonian of an n-dimensional harmonic oscillator where

$$m_n = C, \quad (2.22a)$$

and

$$\omega_n = u_p \cdot k_n. \quad (2.22b)$$

The relation (2.21) shows that the total stored electromagnetic energy in the cavity equals to the sum of the energies stored in the individual modes. This point is consistent with the well known result that in the absence of dissipation no cross coupling among different modes exists [13]; thereby, each mode could be treated independently.

2.3 Quantum Microwave Resonator

In order to quantize the classical Hamiltonian of (2.21), the charge and flux variables must be replaced by corresponding operators. Thus,

$$H = \sum_{n=1}^{\infty} \left[\frac{\hat{Q}_n^2}{2C} + k_n^2 \frac{\hat{\Phi}_n^2}{2L} \right], \quad (2.23)$$

where the following commutation relations hold

$$[\hat{Q}_m, \hat{\Phi}_n] = i\hbar\delta_{mn}, \quad (2.24a)$$

$$[\hat{\Phi}_m, \hat{\Phi}_n] = 0, \quad (2.24b)$$

$$[\hat{Q}_m, \hat{Q}_n] = 0, \quad (2.24c)$$

and δ_{mn} is the Kronecker delta function.

Clearly, if one attempts to quantize an infinite transmission line along the same arguments, the integral (2.17) diverges. Alternatively, points along an infinite transmission line, at a given time t , may be viewed as independent SHOs with their location z playing only the role of an index, similar to what n is doing in (2.23). In that case

$$[\hat{Q}(z, t), \hat{\Phi}(z', t')] = i\hbar\delta(z - z')\delta(t - t'), \quad (2.25a)$$

$$[\hat{\Phi}(z, t), \hat{\Phi}(z', t')] = 0, \quad (2.25b)$$

$$[\hat{Q}(z, t), \hat{Q}(z', t')] = 0, \quad (2.25c)$$

and $\delta(x)$ is the Dirac delta function because the Fourier series must be replaced by Fourier transforms. The boundary conditions at the two ends of a resonator, however, provide

correlations among the points along a resonator, which was exploited by expanding the dynamical variables Φ and Q , or equivalently voltage and current, in terms of the normal modes of the system. The normal modes are, in fact, the collective modes associated with all of the points in the system where the state of any given point uniquely defines the state of all other points. The collective modes attributed to a finite transmission line resonator are the standing waves used as the kernel of the Fourier series in (2.8). The boundary conditions in a resonator establish a one to one correspondence between the resonance frequency ω_n and the wavenumber k_n through (2.22b). In contrast, in an infinite transmission line for any wavenumber k there would be a continuum of frequencies ω , which manifests the absolute independence of the points along an infinite transmission line.

Hence, if one wishes to quantize an infinite transmission line, it must be viewed as an aggregate of connected finite-length resonators with proper boundary conditions such as a periodic boundary condition. This approach is exactly similar to the quantization of traveling light waves in quantum optics. Therefore, what follows as well applies to an infinite transmission line excited by a time harmonic signal. One can verify this point by recovering (2.25) from (2.24) and (2.20) and using the completeness of sine functions.

2.3.1 Diagonalization of the Hamiltonian

To diagonalize the Hamiltonian, the creation and annihilation operators are defined

$$a_n = \left(\frac{k_n}{2\hbar Z_0} \right)^{1/2} \hat{\Phi}_n + i \left(\frac{Z_0}{2\hbar k_n} \right)^{1/2} \hat{Q}_n, \quad (2.26a)$$

$$a_n^\dagger = \left(\frac{k_n}{2\hbar Z_0} \right)^{1/2} \hat{\Phi}_n - i \left(\frac{Z_0}{2\hbar k_n} \right)^{1/2} \hat{Q}_n, \quad (2.26b)$$

and therefore,

$$\hat{H} = \sum_{n=1}^{\infty} \hbar\omega_n \left(a_n^\dagger a_n + \frac{1}{2} \right), \quad (2.27)$$

where

$$[a_m, a_n^\dagger] = \delta_{mn}, \quad (2.28a)$$

$$[a_m, a_n] = 0, \quad (2.28b)$$

$$[a_m^\dagger, a_n^\dagger] = 0. \quad (2.28c)$$

The flux and charge operator, also, can be written in terms of the ladder operators

$$\hat{\Phi}_n = \left(\frac{\hbar Z_0}{2k_n} \right)^{1/2} (a_n^\dagger + a_n), \quad (2.29a)$$

$$\hat{Q}_n = i \left(\frac{\hbar k_n}{2Z_0} \right)^{1/2} (a_n^\dagger - a_n). \quad (2.29b)$$

2.3.2 Uncertainty Relations

We begin to examine the uncertainty relations with $|m, n\rangle$, i.e. an MR whose mode m is in the number state $|n\rangle$. According to the appendix A,

$$\langle \hat{\Phi}_m \rangle = 0, \quad (2.30a)$$

$$\langle \hat{Q}_m \rangle = 0, \quad (2.30b)$$

$$(\Delta \hat{\Phi}_m)^2 = \frac{\hbar Z_0}{k_m} \left(n + \frac{1}{2} \right), \quad (2.30c)$$

$$(\Delta \hat{Q}_m)^2 = \frac{\hbar k_m}{Z_0} \left(n + \frac{1}{2} \right). \quad (2.30d)$$

In terms of the current and voltage operators,

$$\langle \hat{i}_m \rangle = 0, \quad (2.31a)$$

$$\langle \hat{v}_m \rangle = 0, \quad (2.31b)$$

$$(\Delta \hat{i}_m)^2 = \frac{\hbar \omega_m}{L} \left(n + \frac{1}{2} \right), \quad (2.31c)$$

$$(\Delta \hat{v}_m)^2 = \frac{\hbar \omega_m}{C} \left(n + \frac{1}{2} \right). \quad (2.31d)$$

The relations about the averages of the operators show that the dc components of the flux, charge, current, and voltage are zero in the MR for all modes. The uncertainty relations show that, while keeping the phase velocity of the line and thereby the resonance frequency constant, the uncertainty in the charge and current could be reduced by increasing the line's impedance Z_0 , which would be at the expense of increasing the uncertainty in the flux and voltage. Nonetheless the uncertainty product doesn't depend on the line's characteristic impedance and is a fundamental quantum mechanical limit

$$\Delta \hat{\Phi}_m \cdot \Delta \hat{Q}_m = \hbar \left(n + \frac{1}{2} \right), \quad (2.32a)$$

and

$$\Delta \hat{v}_m \cdot \Delta \hat{i}_m = \hbar \omega_m u_p \left(n + \frac{1}{2} \right). \quad (2.32b)$$

The vacuum state of all modes, i.e. $|m, 0\rangle$, are clearly minimum uncertainty states. The uncertainty for the flux, at a given number states, decreases for the higher order modes, whereas the same quantity increases with the mode number for the charge. Nevertheless, the uncertainty product of the flux and charge is independent of the mode number. In contrast, the uncertainty in both current and voltage, at a given number state, as well as

their uncertainty product increase with the mode number, which is because current and voltage are not canonical conjugate variables of the system.

For coherent states $|m, \alpha\rangle$, which more closely represent the actual state of the MR modes in classical experiments, the uncertainty relations follow

$$\langle \hat{\Phi}_m \rangle = \left(\frac{\hbar Z_0}{2k_m} \right)^{1/2} (\alpha + \alpha^*) = \left(\frac{2\hbar Z_0}{k_m} \right)^{1/2} \Re(\alpha), \quad (2.33a)$$

$$\langle \hat{Q}_m \rangle = i \left(\frac{\hbar k_m}{2Z_0} \right)^{1/2} (\alpha^* - \alpha) = \left(\frac{2\hbar k_m}{Z_0} \right)^{1/2} \Im(\alpha), \quad (2.33b)$$

$$(\Delta \hat{\Phi}_m)^2 = \frac{\hbar Z_0}{2k_m}, \quad (2.33c)$$

$$(\Delta \hat{Q}_m)^2 = \frac{\hbar k_m}{2Z_0}. \quad (2.33d)$$

The uncertainty for the flux and charge, for a given coherent state $|\alpha\rangle$, respectively decreases and increases for higher order modes. The uncertainty in either of the two may be squeezed, with adjusting the characteristic impedance, at the price of increasing the uncertainty of the other one. The above relations can be rewritten in terms of the current and voltage operators

$$\langle \hat{i}_m \rangle = \left(\frac{2\hbar\omega_m}{L} \right)^{1/2} \Re(\alpha), \quad (2.34a)$$

$$\langle \hat{v}_m \rangle = \left(\frac{2\hbar\omega_m}{C} \right)^{1/2} \Im(\alpha), \quad (2.34b)$$

$$(\Delta \hat{i}_m)^2 = \frac{\hbar\omega_m}{2L}, \quad (2.34c)$$

$$(\Delta \hat{v}_m)^2 = \frac{\hbar\omega_m}{2C}. \quad (2.34d)$$

The uncertainty products in turn follow

$$\Delta\hat{\Phi}_m \cdot \Delta\hat{Q}_m = \frac{\hbar}{2}, \quad (2.35a)$$

and

$$\Delta\hat{v}_m \cdot \Delta\hat{i}_m = \frac{\hbar\omega_m u_p}{2}. \quad (2.35b)$$

Obviously, the coherent states are minimum uncertainty states for all modes.

2.3.3 Density Matrix

The density operator of the MR can be written as

$$\hat{\rho} = \hat{\rho}_1 \otimes \hat{\rho}_2 \otimes \dots \otimes \hat{\rho}_n, \quad (2.36)$$

where $\hat{\rho}_n$ is density operator associated with the mode n . According to (2.28), the commutation relation among $\hat{\rho}_n$ is

$$[\hat{\rho}_m, \hat{\rho}_n] = 0, \quad (2.37)$$

therefore the time evolution of the density operator for each mode may be written independently

$$\dot{\hat{\rho}}_n = i\omega_n(a_n^\dagger a_n \hat{\rho}_n - \hat{\rho}_n a_n^\dagger a_n). \quad (2.38)$$

Similar to the density operator of an LC resonator, $\hat{\rho}_n$ can be expanded as a P-representation

$$\hat{\rho}_n = \int P_n(\alpha_n, \alpha_n^*, t) |n, \alpha_n\rangle \langle n, \alpha_n| d^2\alpha_n. \quad (2.39)$$

Referring to (1.37) in the previous chapter, for a mode starting from a coherent state $|\alpha_{n0}\rangle$

$$P_n(\alpha_n, \alpha_n^*, t) = \delta^2(\alpha_n - \alpha_{n0}e^{+i\omega_n t}), \quad (2.40)$$

thus

$$|\psi(t)\rangle = \sum_{n=1}^{\infty} |n, \alpha_{n0}\rangle e^{i\omega_n t}. \quad (2.41)$$

2.4 Quantum Damped Microwave Resonator

Since each mode of an MR corresponds to an independent SHO, the damping for each mode can be treated individually as the interaction with a reservoir through the following interaction Hamiltonian:

$$\mathcal{V}_n = \hbar \sum_k g_{nk} [b_k^\dagger a_n e^{-i(\omega_n - \omega_k)t} + a_n^\dagger b_k e^{i(\omega_n - \omega_k)t}], \quad (2.42)$$

where ω_n is the resonance frequency of the n 'th mode, ω_k and g_k respectively are the eigenfrequency and the coupling factor of the mode \mathbf{k} in the reservoir, and b_k^\dagger and b_k are the corresponding creation and annihilation operators of the reservoir modes.

2.4.1 Field Damping and Fokker-Planck Equation

Similar to the discussion of the previous chapter, the equation of motion for the reduced density matrix of the n th mode is

$$\begin{aligned} \dot{\hat{\rho}}_n = & - \frac{\eta_n}{2} \bar{n}_{th,n} (a_n a_n^\dagger \hat{\rho}_n - 2a_n^\dagger \hat{\rho}_n a_n + \hat{\rho}_n a_n a_n^\dagger) \\ & - \frac{\eta_n}{2} (\bar{n}_{th,n} + 1) (a_n^\dagger a_n \hat{\rho}_n - 2a_n \hat{\rho}_n a_n^\dagger + \hat{\rho}_n a_n^\dagger a_n), \end{aligned} \quad (2.43)$$

where η_n is the damping constant attributed to the n 'th mode, which is related to the quality factor of the n 'th mode as $\eta_n = \omega_n/Q_n$, and $\bar{n}_{th,n}$ is the mean number of quanta, at the frequency ω_n , in the thermal reservoir [9],

$$\bar{n}_{th,n} = \frac{1}{\exp\left(\frac{\hbar\omega_n}{k_B T} - 1\right)} \quad (2.44)$$

Within the P-representation, the following Fokker-Plank equation governs the dynamics of the damped mode,

$$\dot{P}_n = \frac{\eta}{2} \left(\frac{\partial}{\partial \alpha_n} \alpha_n + \frac{\partial}{\partial \alpha_n^*} \alpha_n^* \right) P_n + \eta_n \bar{n}_{th} \frac{\partial^2 P_n}{\partial \alpha_n \partial \alpha_n^*}. \quad (2.45)$$

Upon starting from a coherent state $|n, \alpha_{n0}\rangle$,

$$P_n(\alpha_n, \alpha_n^*, 0) = \delta^2(\alpha_n - \alpha_{n0}), \quad (2.46)$$

and (2.45) gives

$$P_n(\alpha_n, \alpha_n^*, t) = \frac{1}{\pi D_n(t)} \exp\left[-\frac{|\alpha_n - \alpha_{n0} U_n(t)|^2}{D_n(t)}\right], \quad (2.47)$$

where

$$D_n(t) = \bar{n}_{th,n} (1 - e^{-\eta_n t}), \quad (2.48a)$$

and

$$U_n(t) = e^{-\eta_n t/2 - i\omega_n t}. \quad (2.48b)$$

2.4.2 Uncertainty Relations

Using the density operator of the damped mode, it is straightforward to show that starting from a coherent state $|n, \alpha_n\rangle$,

$$\langle \hat{\Phi}_n \rangle = \left(\frac{2\hbar Z_0}{k_m} \right)^{1/2} [|\alpha_n| e^{-\eta n t/2} \cos(\omega_n t - \phi_n)], \quad (2.49a)$$

and

$$\langle \hat{Q}_n \rangle = \left(\frac{2\hbar k_m}{Z_0} \right)^{1/2} [-|\alpha_n| e^{-\eta n t/2} \sin(\omega_n t - \phi_n)], \quad (2.49b)$$

where $\alpha_n = |\alpha_n| e^{i\phi_n}$. Moreover,

$$(\Delta \hat{\Phi}_n)^2 = \frac{\hbar Z_0}{2k_m} [1 + 2D_n(t)], \quad (2.50a)$$

and

$$(\Delta \hat{Q}_n)^2 = \frac{\hbar k_m}{2Z_0} [1 + 2D_n(t)]. \quad (2.50b)$$

According to (2.48) and $D_n(0) = 0$, the uncertainties of the conjugate variables start from that of a lossless mode and increases in time.

2.5 Summary and Discussion

This chapter studied the quantization of a microwave resonator (MR). Based on the equivalent circuit model of a transmission line (TL), every single point along the MR was modeled by an LC resonator. The differential Lagrangian and Hamiltonian functions, in turn, were obtained by making a correspondence between the electric and magnetic energies to the kinetic and potential energies, respectively. It turned out that the magnetic flux in the transverse plane Φ and the electric charge Q were the canonically conjugate variables. The

system's total Lagrangian and Hamiltonian, then, were obtained by integration over the length of the resonator. Given the finite length of the MR, the flux and charge variables were expanded as Fourier series, in terms of spatial standing-waves satisfying the proper boundary conditions imposed by the line terminations, where the Hamiltonian cast into that of an infinite number of independent SHOs with a mass of $m = C$, the capacitance per unit length of the TL, and a resonance frequency $\omega_n = k_n \cdot u_p$ corresponding to different modes of the MR. By applying the standard quantization recipe, the quantum Hamiltonian operator was found with the charge \hat{Q}_n and flux $\hat{\Phi}_n$ associated with each mode being the conjugate operators \hat{p}_n and \hat{q}_n . Next, the Hamiltonian was diagonalized through the introduction of the ladder operators a_n and a_n^\dagger , and the averages and uncertainty relations for the flux, charge, voltage, and current operators were found for the each modes in the number state $|m, n\rangle$ and the coherent state $|m, \alpha_m\rangle$. Through the time evolution of the density operator of each mode $\hat{\rho}_n$, it was shown that a mode starting at a coherent state $|n, \alpha_{n0}\rangle$ will evolve in time as $|n, \alpha_{n0}e^{i\omega_n t}\rangle$. Similar to an RLC resonator, the mode damping was modeled as the coupling of the lossless mode into a thermal bath of SHOs. Applying the same quantum optical approach as in the previous chapter, the Fokker-Planck equation associated with the P-representation of each mode was derived, which showed that for a mode starting from $|n, \alpha_{n0}\rangle$ the P-representation starts from a delta function and broadens in time as a Gaussian wave-packet and moves along an exponential spiral towards the vacuum state $|n, 0\rangle$. The time evolution of the averages and uncertainties of the charge and flux operators was formulated accordingly, wherein each mode exhibited the same behavior as of an RLC resonator.

A microwave resonator, in general, realizes electromagnetic SHOs with a high resonance frequency. In accordance with (1.62), this high frequency oscillator lends itself more conveniently to experiments than a simple LC resonator because of its robustness against thermal

fluctuations. However, a microwave resonator produces an infinite number of SHOs in the form of higher order resonant modes, which, though ideally independent, are vulnerable to cross coupling with a slight nonlinearity in the structure such as the material nonlinearity and dispersion. Inasmuch as superconductors exhibit little nonlinearity and dispersion for microwave frequencies, well below their energy gap, superconducting cavities seem to be the ultimate candidate for operation at the quantum limit.

Chapter 3

Josephson Anharmonic Resonator

3.1 Introduction

In the previous chapters, it was shown that the eigenstates of a harmonic electromagnetic resonator, whether in the form of a lumped-element LC circuit or a microwave cavity, are pure number states, which are equally spaced in the energy space. Therefore, these devices are located at the edge of the correspondence limit where photons with an energy corresponding to the system's classical resonance frequency can stimulate and couple to all of the quantum states. To be able to address each quantum state individually, a resonator whose eigenstates are unequally spaced in energy, namely an anharmonic electromagnetic oscillator, is required. As such, a nonlinear device should be utilized to produce the desired anharmonicity, and appropriate harmonic resonators can be used, as photon banks, to address different levels of the system [14].

Josephson junctions are prominent candidates for implementation of anharmonic oscillators not only because of their intrinsic nonlinearity, but also because of their low loss and controllability. We begin this chapter by reviewing the phenomenology of Josephson

tunneling using a two-level system approach [15]. Based on the resistively and capacitively shunted junction model (RCSJ), we will review the classical dynamics of both unbiased and driven Josephson junction, where the associated Lagrangian and Hamiltonian functionals as well as their anharmonicity are derived. After quantizing the Hamiltonian, the anharmonic oscillator will be treated by means of perturbation method, where eigenenergies of the system are obtained and eigenstates are expanded in terms of pure number states. Treatment of the effects of dissipation in a Josephson resonator is postponed until a subsequent chapter, thus, throughout this chapter the devices are assumed to be lossless.

3.2 Josephson Tunneling

According to the BCS theory [16], electrons in a superconductor form Cooper pairs, i.e. electron pairs with a charge e^* and mass m_0^* twice as the charge e and mass m_0 of a normal electron, wherein all the pairs condense into a macrostate $|s\rangle$. For many problems, a phenomenological approach, based on a macroscopic wavefunction attributed to the macrostate $|s\rangle$, is very illustrative [15, 17, 18]:

$$\Psi(\mathbf{r}) = \rho(\mathbf{r})^{1/2} e^{i\varphi(\mathbf{r})}, \quad (3.1)$$

where

$$\rho(\mathbf{r}) = \langle s | \Psi^* \Psi | s \rangle \quad (3.2)$$

is the population density of the Cooper pairs over the specimen. The electric current density, in the presence of a magnetic vector potential \mathbf{A} , follows¹

$$\mathbf{J} = \frac{e^*}{m_0^*} \left[\frac{i\hbar}{2} (\Psi \nabla \Psi^* - \Psi^* \nabla \Psi) - e^* \mathbf{A} |\Psi|^2 \right], \quad (3.3)$$

therefor by using (3.1),

$$\mathbf{J} = \rho \frac{e}{m_0} (\hbar \nabla \varphi - 2e \mathbf{A}). \quad (3.4)$$

Gauge invariance requires that under the transformation

$$\mathbf{A} \rightarrow \mathbf{A} + \nabla \chi \quad \text{and} \quad U \rightarrow U - \frac{\partial \chi}{\partial t}, \quad (3.5)$$

where U is the electrostatic potential, the phase also transforms as [15]

$$\varphi \rightarrow \varphi + \frac{2e}{\hbar} \chi, \quad (3.6)$$

to keep the observable quantities unchanged. As usual, the time evolution of Ψ in the stationary conditions is determined by the time-independent Schrodinger equation,

$$i\hbar \frac{\partial \Psi}{\partial t} = E \Psi. \quad (3.7)$$

Now, imagine that two separate superconducting samples $|L\rangle$ and $|R\rangle$, whose wavefunctions respectively are Ψ_L and Ψ_R , are brought into close proximity, so that the tails of their individual wavefunctions overlap, as shown in Fig. 3.1. Therefore, the overall

¹The equation is written in the SI unit system.

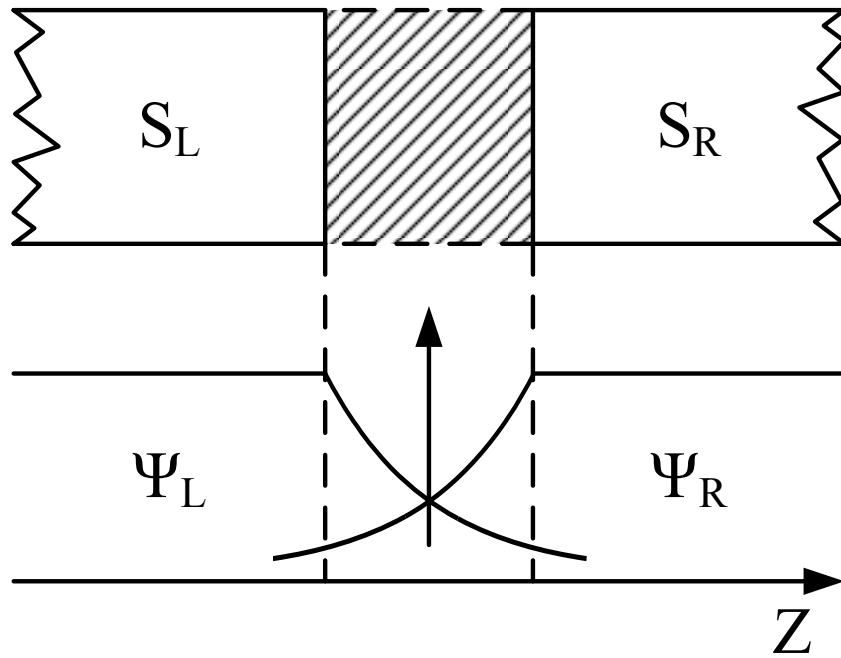


Figure 3.1: Overlap of the macroscopic wavefunction in a Josephson junction.

wavefunction of the system may be written as

$$\Psi = \Psi_L|L\rangle + \Psi_R|R\rangle. \quad (3.8)$$

The Hamiltonian of the system reads

$$H = H_L + H_T + H_R, \quad (3.9)$$

where

$$H_L = E_L|L\rangle\langle L|, \quad (3.10a)$$

$$H_R = E_R|R\rangle\langle R|, \quad (3.10b)$$

and the interaction Hamiltonian is

$$H_T = K|L\rangle\langle R| + K|R\rangle\langle L|, \quad (3.11)$$

where K is the interaction amplitude between the two samples, and can be assumed to be real in the absence of \mathbf{A} [15]. The interaction Hamiltonian accounts for the tunneling of Cooper pairs across the junction, which is the renowned Josephson phenomenon. If it is further assumed that there is a potential difference V between the two samples,

$$E_L - E_R = 2eV, \quad (3.12)$$

the Schrodinger equation for the system reads

$$i\hbar\frac{\partial\Psi_L}{\partial t} = eV\Psi_L + K\Psi_R, \quad (3.13a)$$

and

$$i\hbar \frac{\partial \Psi_R}{\partial t} = -eV \Psi_R + K \Psi_L. \quad (3.13b)$$

By replacing the explicit form of the wavefunctions (3.1) and separating the real and imaginary parts, it is straightforward to show that

$$J = J_c \sin \varphi, \quad (3.14a)$$

and

$$\frac{\partial \varphi}{\partial t} = \frac{2eV}{\hbar}, \quad (3.14b)$$

where J is the current density defined as

$$J \equiv \frac{\partial \rho_L}{\partial t} = -\frac{\partial \rho_R}{\partial t}, \quad (3.15)$$

φ is the phase difference of the macrostates across the junction

$$\varphi = \varphi_L - \varphi_R, \quad (3.16)$$

and J_c is the critical current density,

$$J_c \equiv \frac{2K}{\hbar} \sqrt{\rho_L \rho_R}. \quad (3.17)$$

Equation set (3.14) gives the equation of motions of a superconducting weaklink, wherein the tunneling of Cooper pairs are at work.

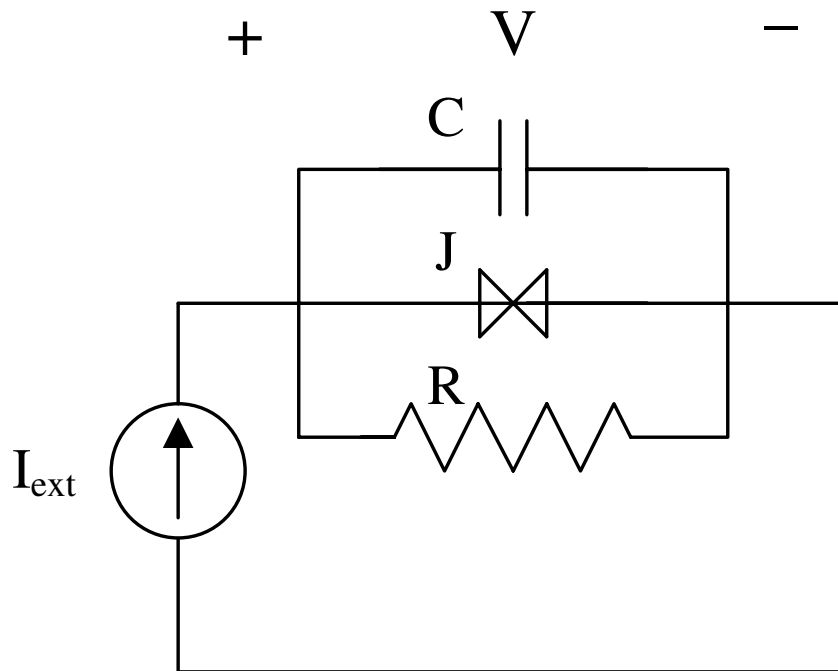


Figure 3.2: RCSJ equivalent circuit model of a biased Josephson junction.

3.3 Classical Dynamics of Josephson Junction

In practice, real Josephson devices and weaklinks are subjected to a parasitic capacitance arising from the charge accumulation across the junction, which depends on the materials and geometry of the device. Moreover, the tunneling mechanism may be dissipative, which together with the stray resistance of the circuit, could be modeled as a shunt resistor. Therefore, a real Josephson junction can be represented by the circuit of Fig. 3.2, known as the resistively and capacitively shunted junction (RCSJ) model [15]. Here, we assume that the value of the capacitance remains constant for all frequencies, i.e. there is no dispersion. However, a dispersive Josephson junction has been studied in [19].

The KCL equation in the circuit yields

$$C \frac{\partial v}{\partial t} + \frac{v}{R} + I_c \sin \varphi = I_0, \quad (3.18)$$

where I_0 is the bias current, and I_c is the critical current of the Josephson junction. Using Josephson junction's basic equation set (3.14), the equation of motion of the system can be written

$$C \left(\frac{\Phi_0}{2\pi} \right) \frac{\partial^2 \varphi}{\partial t^2} + \frac{1}{R} \left(\frac{\Phi_0}{2\pi} \right) \frac{\partial \varphi}{\partial t} + I_c \sin \varphi = I_0, \quad (3.19)$$

where Φ_0 is the magnetic flux quanta:

$$\Phi_0 \equiv \frac{h}{2e}. \quad (3.20)$$

Equation (3.19) represents² the motion of a body of mass m ,

$$m = C \left(\frac{\Phi_0}{2\pi} \right)^2, \quad (3.21)$$

along the φ axis within a potential field U ,

$$U(\varphi) = - \left(\frac{\Phi_0 I_c}{2\pi} \right) \cos \varphi - \left(\frac{\Phi_0 I_0}{2\pi} \right) \varphi, \quad (3.22)$$

at the presence of a dragging force $\frac{1}{R} \left(\frac{\Phi_0}{2\pi} \right)^2 \frac{\partial \varphi}{\partial t}$.

The potential (3.22) is called the “tilted washboard” potential, and is illustrated in Fig.

²Note that to establish the aforementioned analogy, multiplication of (3.19) by a factor of $\left(\frac{\Phi_0}{2\pi} \right)$ is necessary for U to have the unit of energy.

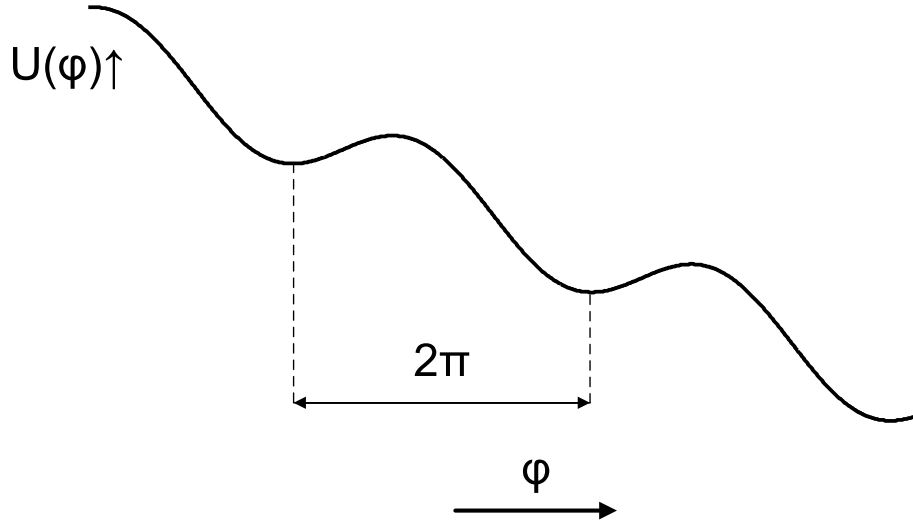


Figure 3.3: Tilted washboard potential associated with a Josephson junction.

3.3. For $I_0 < I_c$, the potential has local minima at points

$$\varphi_m = \sin^{-1} \left(\frac{I_0}{I_c} \right) + 2n\pi \quad (\text{integer } n), \quad (3.23)$$

whereas for $I_0 = I_c$ the minima turn into inflection points. For $I_0 > I_c$, there is no minima, and the system is called to be in the voltage state. For an isolated Josephson junction, i.e. $I_0 = 0$, and in the absence of dissipation, i.e. $R \rightarrow \infty$, the equation of motion reduces to

$$\frac{\partial^2 \varphi}{\partial t^2} + \left(\frac{2\pi I_c}{C\Phi_0} \right) \sin \varphi = 0. \quad (3.24)$$

At the bottom of the well, the fluctuations of φ are very small such that $\sin \varphi \approx \varphi$.

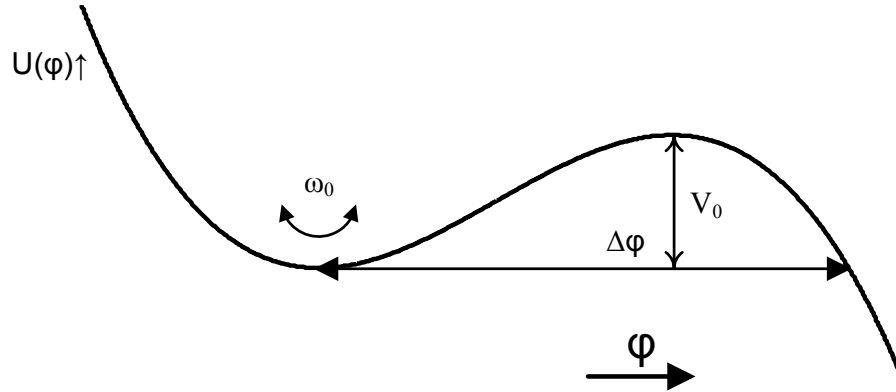


Figure 3.4: Cubic approximation to the tilted washboard potential of a Josephson junction under small bias around its minimum .

Therefore, (3.24) corresponds to oscillations of the φ at the plasma frequency ω_p , where

$$\omega_p \equiv \left(\frac{2\pi I_c}{C\Phi_0} \right)^{1/2}. \quad (3.25)$$

Increasing the bias current and the particle eventually escapes from the well and moves down the washboard potential; thus, the average voltage is no longer zero.

At a bias current $I_0 = I_c - \delta I$ where $\delta I \ll I_c$, the minimum of the potential U obviously happens at

$$\varphi_m = \sin^{-1}(1 - x), \quad (3.26)$$

where

$$x \equiv \left(\frac{\delta I}{I_c} \right) \ll 1. \quad (3.27)$$

One can expand U around φ_m , where the dc term could be neglected, because the origin

of potential is arbitrary, and $\frac{\partial U}{\partial \varphi} \Big|_{\varphi_m} = 0$, because φ_m is a minimum of U . Therefore,

$$\begin{aligned} U(\varphi) &\simeq \frac{1}{2} \frac{\partial^2 U}{\partial \varphi^2} (\varphi - \varphi_m)^2 + \frac{1}{6} \frac{\partial^3 U}{\partial \varphi^3} (\varphi - \varphi_m)^3 \\ &= \frac{1}{2} m \omega_0^2 \varphi^2 + \frac{1}{6} \frac{\partial^3 U}{\partial \varphi^3} \varphi^3, \end{aligned} \quad (3.28)$$

where

$$\omega_0^2 \equiv m^{-1} \frac{\partial^2 U}{\partial \varphi^2} \Big|_{\varphi_m}, \quad (3.29)$$

and the mass m is given by (3.21). Hence, the tilted washboard potential for a Josephson junction under small bias can be approximated by the following cubic potential around its minimum, as is illustrated by Fig. 3.4,

$$U(\varphi) = \frac{1}{2} m \omega_0^2 \varphi^2 \left(1 - \frac{\varphi}{\Delta \varphi} \right), \quad (3.30a)$$

where

$$m = C \left(\frac{\Phi_0}{2\pi} \right)^2, \quad (3.30b)$$

$$\omega_0 = \omega_p \sqrt{2x} = \left(\frac{2\pi I_c}{C \Phi_0} \right)^{1/2} \left(2 \frac{\delta I}{I_c} \right)^{1/2}, \quad (3.30c)$$

and

$$\Delta \varphi = \left(18 \frac{\delta I}{I_c} \right)^{1/4}. \quad (3.30d)$$

According to Fig. 3.4, the height of the potential barrier in the cubic potential is

$$V_0 = \frac{2}{27} m \omega_0^2 (\Delta \varphi)^2 = \frac{2\sqrt{2}}{3\pi} \Phi_0 I_c \left(\frac{\delta I}{I_c} \right)^{3/2}. \quad (3.31)$$

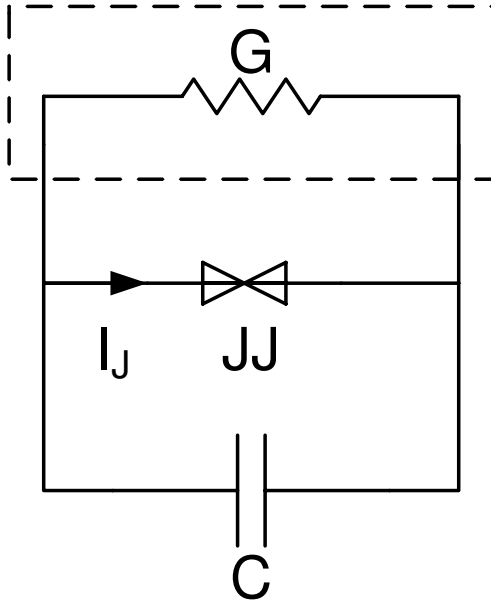


Figure 3.5: RCSJ equivalent circuit model of an unbiased Josephson junction.

3.3.1 The Lagrangian and Hamiltonian of Unbiased Josephson Resonator

For an unbiased Josephson junction as illustrated in Fig. 3.5, the equation of motion (3.19) simply reduces to

$$C \left(\frac{\Phi_0}{2\pi} \right)^2 \frac{\partial^2 \varphi}{\partial t^2} + \left(\frac{\Phi_0 I_c}{2\pi} \right) \sin \varphi = 0. \quad (3.32)$$

The energy stored in the junction is obtained as follows:

$$\begin{aligned}
E &= \int_0^t i(\tau)v(\tau)d\tau \\
&= \int_0^{\varphi(t)} \left(\frac{\Phi_0 I_c}{2\pi} \right) \sin \varphi d\varphi \\
&= \left(\frac{\Phi_0 I_c}{2\pi} \right) [1 - \cos \varphi] = E_J [1 - \cos \varphi].
\end{aligned} \tag{3.33}$$

In the above equations we assumed $\varphi(0) = 0$ in order to impose $E_J = 0$ for $\varphi = 2n\pi$, where the current is zero.

The Lagrangian

The equation of motion (3.32) is resulted from the Lagrangian

$$\mathcal{L} = \frac{1}{2}C \left(\frac{\Phi_0}{2\pi} \right)^2 \left(\frac{\partial\varphi}{\partial t} \right)^2 - \left(\frac{\Phi_0 I_c}{2\pi} \right) [1 - \cos \varphi], \tag{3.34}$$

when φ is taken as the independent variable q . Clearly, the electric energy stored in the capacitor corresponds to the kinetic energy, whereas the energy stored in the Josephson junction resembles the potential energy. Therefore,

$$p \equiv \frac{\partial\mathcal{L}}{\partial\dot{\varphi}} = C \left(\frac{\Phi_0}{2\pi} \right)^2 \left(\frac{\partial\varphi}{\partial t} \right) \tag{3.35}$$

$$= \hbar \left(\frac{Cv}{2e} \right), \tag{3.36}$$

which shows that the canonical momentum conjugate to the independent variable φ is proportional to the number of Cooper pairs accumulated at the junction.

The Hamiltonian

One can find the Hamiltonian of the unbiased Josephson junction system through the Lagrangian (3.34), where

$$\begin{aligned}\mathcal{H} &= \frac{1}{2}C \left(\frac{\Phi_0}{2\pi}\right)^2 \left(\frac{\partial\varphi}{\partial t}\right)^2 + \left(\frac{\Phi_0 I_c}{2\pi}\right) [1 - \cos\varphi] \\ &= \frac{p^2}{2m} + E_J [1 - \cos\varphi].\end{aligned}\tag{3.37}$$

3.3.2 The Lagrangian and Hamiltonian of Driven Josephson Resonator

In the absence of dissipation, the equation of motion for a driven Josephson junction reads

$$C \left(\frac{\Phi_0}{2\pi}\right)^2 \frac{\partial^2\varphi}{\partial t^2} + \left(\frac{\Phi_0 I_c}{2\pi}\right) \sin\varphi = \left(\frac{\Phi_0 I_0}{2\pi}\right).\tag{3.38}$$

The Lagrangian

The equation of motion (3.38) is recovered from the following Lagrangian when as before φ is taken as the independent variable,

$$\begin{aligned}\mathcal{L} &= \frac{1}{2}C \left(\frac{\Phi_0}{2\pi}\right)^2 \left(\frac{\partial\varphi}{\partial t}\right)^2 - U(\varphi) \\ &= \frac{1}{2}C \left(\frac{\Phi_0}{2\pi}\right)^2 \left(\frac{\partial\varphi}{\partial t}\right)^2 + \left(\frac{\Phi_0 I_c}{2\pi}\right) \cos\varphi + \left(\frac{\Phi_0 I_0}{2\pi}\right) \varphi,\end{aligned}\tag{3.39}$$

where U is the tilted washboard potential defined in (3.22). Clearly, the electric energy stored in the capacitor corresponds to the kinetic energy, and tilted washboard potential of the Josephson junction resembles the potential energy. The canonical momentum con-

jugate to the independent variable φ is again proportional to the number of Cooper pairs accumulated at the junction:

$$p \equiv \frac{\partial \mathcal{L}}{\partial \dot{\varphi}} = C \left(\frac{\Phi_0}{2\pi} \right)^2 \left(\frac{\partial \varphi}{\partial t} \right) \quad (3.40)$$

$$= \hbar \left(\frac{Cv}{2e} \right). \quad (3.41)$$

This fact shows that the amplitude and phase of the macroscopic wavefunction (3.1) are, in fact, conjugate variables, and there is always an uncertainty implicit in the definition of such a wavefunction.

The Hamiltonian

It is straightforward to find the Hamiltonian of the driven Josephson junction system from its Lagrangian (3.39):

$$\begin{aligned} \mathcal{H} &= \frac{1}{2} C \left(\frac{\Phi_0}{2\pi} \right)^2 \left(\frac{\partial \varphi}{\partial t} \right)^2 + U(\varphi) \\ &= \frac{1}{2} C \left(\frac{\Phi_0}{2\pi} \right)^2 \left(\frac{\partial \varphi}{\partial t} \right)^2 - \left(\frac{\Phi_0 I_c}{2\pi} \right) \cos \varphi - \left(\frac{\Phi_0 I_0}{2\pi} \right) \varphi. \end{aligned} \quad (3.42)$$

Now, if one approximates the titled washboard potential, around its minimum, by the cubic potential of (3.30), the Hamiltonian can be rewritten as

$$\mathcal{H} = \frac{1}{2} m \left(\frac{\partial \varphi}{\partial t} \right)^2 + \frac{1}{2} m \omega_0^2 \varphi^2 \left(1 - \frac{\varphi}{\Delta \varphi} \right). \quad (3.43)$$

3.4 Quantization of Unbiased Josephson Resonator

According to (3.37), the Hamiltonian operator for the unbiased Josephson system reads

$$H = \frac{\hat{p}^2}{2m} + E_J[1 - \cos \hat{q}], \quad (3.44)$$

where

$$\hat{q} = \hat{\phi}, \quad (3.45a)$$

and

$$\hat{p} = m \frac{\partial \hat{\phi}}{\partial t}. \quad (3.45b)$$

At the bottom of the potential well, where ϕ is small, the potential can be approximated as a quartic potential; therefore,

$$H = \frac{\hat{p}^2}{2m} + \frac{1}{2}m\omega_p^2\hat{q}^2 - \frac{1}{24}m\omega_p^2\hat{q}^4, \quad (3.46)$$

where ω_p is the plasma frequency given by (3.25). The minus sign in the quartic term implies that the anharmonic potential is weaker than a harmonic potential, therefore, the energy separation between adjacent levels must be less than $\hbar\omega_p$. One can account for the quartic term as a perturbation. By introducing the familiar ladder operators in the Appendix A, the Hamiltonian is written as

$$H = H_0 + H_1, \quad (3.47a)$$

where

$$H_0 = \hbar\omega_p \left(a^\dagger a + \frac{1}{2} \right), \quad (3.47b)$$

and

$$\begin{aligned}
H_1 &= -\hbar\kappa(a^\dagger + a)^4 \\
&= -\hbar\kappa \left\{ 2 [(a^{\dagger 2}N + Na^2) + (a^2N + Na^{\dagger 2}) + (a^{\dagger 2} + a^2)] \right. \\
&\quad \left. + (a^{\dagger 4} + a^4) + (6N^2 + 6N + 3) \right\}, \tag{3.47c}
\end{aligned}$$

wherein

$$\kappa \equiv \frac{\hbar}{96m} = \frac{e^2}{24\hbar C}. \tag{3.47d}$$

Here, we assume that $\psi_n^0 = |n\rangle$ and $E_n^0 = \hbar\omega_p(n + 1/2)$ are the eigenfunctions and the eigenenergies of the unperturbed system, whereas ψ_n^1 and $E_n^1 = E_n^0 + W_n$ are those of the perturbed system. By first order perturbation,

$$W_n = \langle n|H_1|n\rangle = -\hbar\kappa (6n^2 + 6n + 3), \tag{3.48}$$

and

$$\begin{aligned}
\psi_n^1 &= A_n[|n\rangle + b_{n,4}^+|n+4\rangle + b_{n,2}^+|n+2\rangle \\
&\quad + b_{n,2}^-|n-2\rangle + b_{n,4}^-|n-4\rangle], \tag{3.49}
\end{aligned}$$

where

$$b_{n,4}^+ = \frac{\kappa}{4\omega_p} [(n+1)(n+2)(n+3)(n+4)]^{1/2}, \quad (3.50a)$$

$$b_{n,2}^+ = \frac{\kappa}{\omega_p} (2n+3) [(n+1)(n+2)]^{1/2}, \quad (3.50b)$$

$$b_{n,2}^- = \frac{-\kappa}{\omega_p} (2n-1) [n(n-1)]^{1/2}, \quad (3.50c)$$

$$b_{n,4}^- = \frac{-\kappa}{4\omega_p} [n(n-1)(n-2)(n-3)]^{1/2}, \quad (3.50d)$$

and

$$A_n = [1 + (b_{n,4}^-)^2 + (b_{n,2}^-)^2 + (b_{n,2}^+)^2 + (b_{n,4}^+)^2]^{-1/2}. \quad (3.50e)$$

The energy of any eigenstate of the unbiased Josephson resonator is always less than the energy of the corresponding level of an SHO. This point is evident from the sign of the W_n as well as the sign of H_1 . In addition, (3.48) shows that the deviation from harmonicity increases for higher order levels, as illustrated in Fig. 3.6. Moreover, the energy separation between adjacent levels is always less than the energy quanta of the corresponding SHO $\hbar\omega_p$, and, in fact, the levels become closer for higher order eigenstates, as shown in Fig. 3.7. The only nonzero terms in the first order expansion of the perturbed eigenstates (3.49) are only those ± 2 or ± 4 away from the unperturbed state. The fidelity of the perturbed eigenstate to pure number states of an SHO is depicted in Fig. 3.8. It is obvious that deviation of the low order levels from the corresponding unperturbed state is small, whereas the high order levels asymptotically approach to the superposition of two number states, respectively ± 2 away from the unperturbed eigenstates.

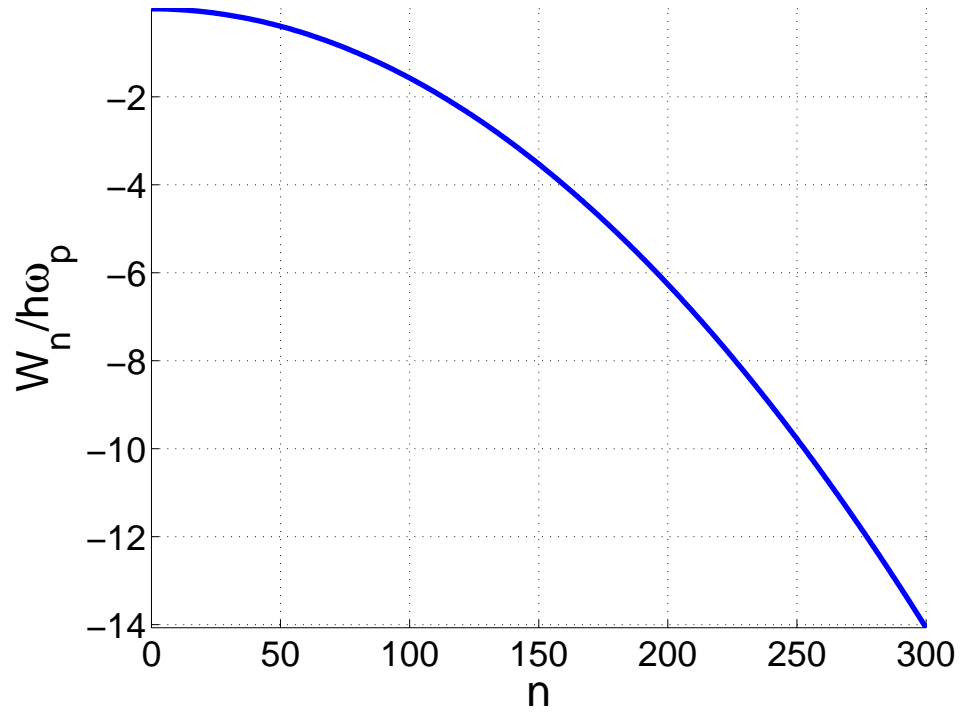


Figure 3.6: Deviation of the eigenenergies from that of an SHO for an unbiased Josephson resonator with $I_c=200\mu A$ and $C =0.5\text{pF}$.

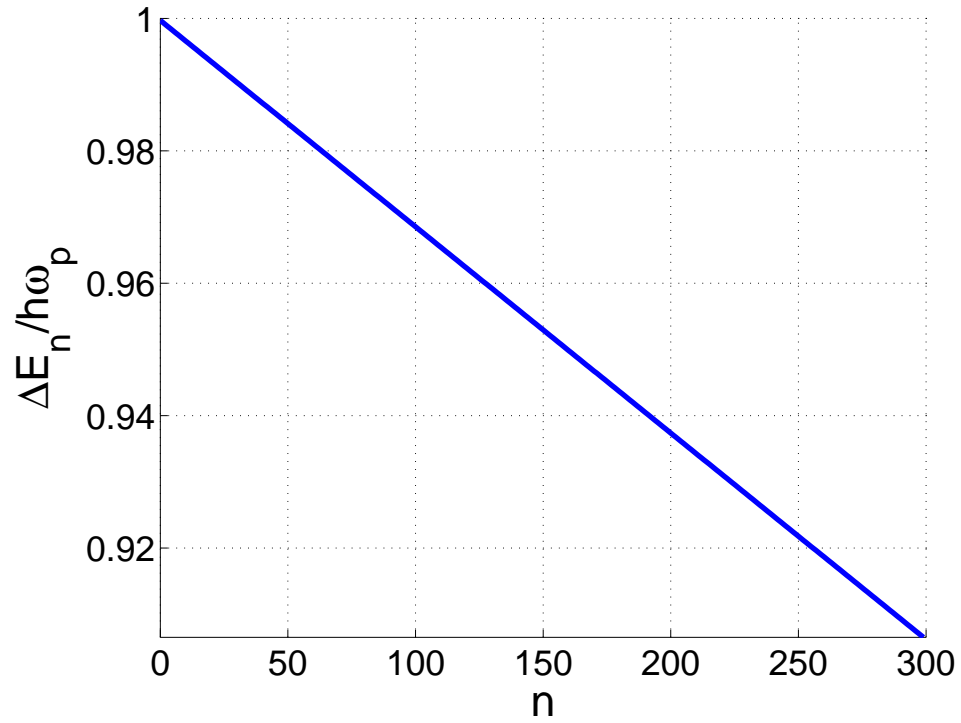


Figure 3.7: The energy separation between adjacent eigenstates of an unbiased Josephson resonator with $I_c=200\mu A$ and $C =0.5\text{pF}$.

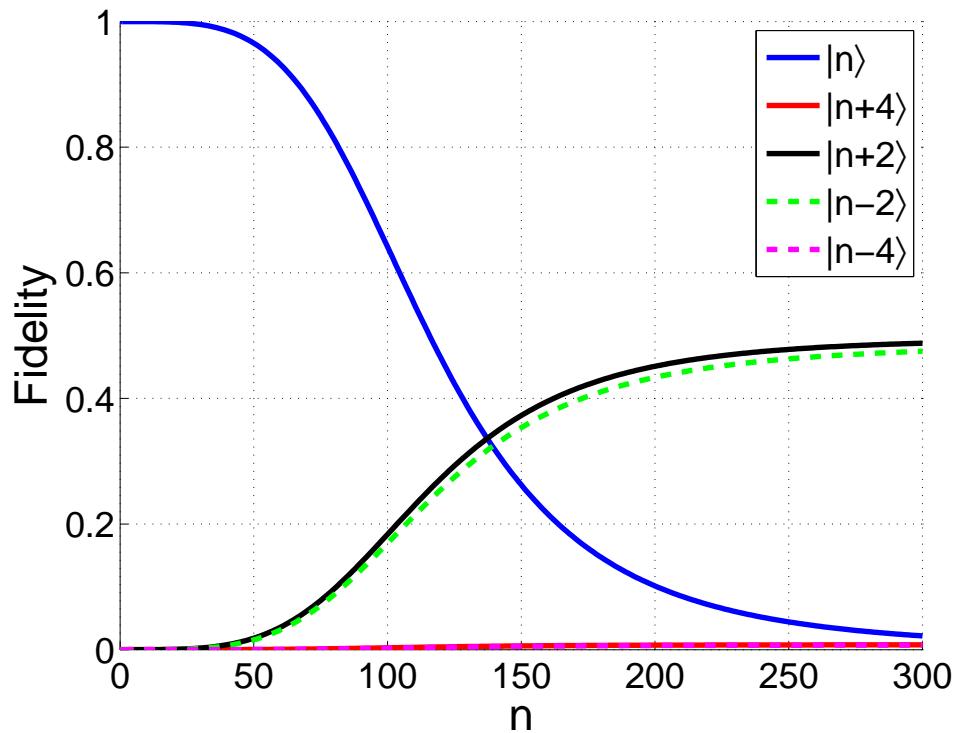


Figure 3.8: The fidelity to pure number states for the eigenstates of an unbiased Josephson resonator with $I_c=200\mu A$ and $C =0.5\text{pF}$.

3.5 Quantization of Driven Josephson Resonator

According to (3.43), the Hamiltonian operator for the driven Josephson system reads

$$H = \frac{\hat{p}^2}{2m} + \frac{1}{2}m\omega_0^2\hat{q}^2 \left(1 - \frac{\hat{q}}{\Delta\varphi}\right), \quad (3.51)$$

where

$$\hat{q} = \hat{\varphi}, \quad (3.52a)$$

and

$$\hat{p} = m \frac{\partial \hat{\varphi}}{\partial t}. \quad (3.52b)$$

Note that the resonance frequency ω_0 , defined in (3.30), differs from the plasma frequency ω_p , due to the applied bias. The minus sign in the cubic term implies that the anharmonic potential is again weaker than a harmonic potential, therefore, the energy separation between adjacent levels must be less than $\hbar\omega_0$.

It is again possible to regard the cubic term as a perturbation and diagonalize the Hamiltonian by the ladder operators:

$$H = H_0 + H_1, \quad (3.53a)$$

where

$$H_0 = \hbar\omega_0 \left(a^\dagger a + \frac{1}{2} \right), \quad (3.53b)$$

and

$$\begin{aligned} H_1 &= -\hbar\lambda(a^\dagger + a)^3 \\ &= -\hbar\lambda \left\{ (a^{\dagger 3} + a^3) + 3(a^\dagger a a^\dagger + a a^\dagger a) \right\}, \end{aligned} \quad (3.53c)$$

wherein

$$\lambda \equiv \frac{1}{4\Delta\varphi} \sqrt{\frac{\hbar\omega_0}{2m}}. \quad (3.53d)$$

clearly λ is independent of bias $\frac{\delta I}{I_c}$. To the first order perturbation, the energy levels of the system is the same as that of an SHO because the perturbation Hamiltonian does not have any term that conserves the number. Nevertheless, the eigenstates are different. One may try a second order perturbation to find results similar those of the previous section; however, for a driven Josephson resonator the quantity of interest is the tunneling rate from the metastable states to the continuum down the tilted-washboard potential which correspond to a voltage state. This is the reason that many researchers have employed the WKB method to study this problem [20]. Here, we do not repeat the calculations for the lossless case, and postpone the discussion to the next chapter where a precise account of macroscopic tunneling along with the effect of dissipation on it are presented.

3.6 Summary and Discussions

This chapter studied Josephson anharmonic resonator as a viable means for the realization of an electrical circuit with non-equidistant quantum levels. The two-level system phenomenology of Josephson tunneling was reviewed, where the overlap of the macroscopic wavefunctions of the superconducting condensates for the two superconducting islands, at the two sides of the junction, results in pair tunneling. The classical dynamics of Josephson resonator, then, was formulated based on the RCSJ model. It was shown that a Josephson resonator corresponds to a mass $C \left(\frac{\Phi_0}{2\pi}\right)^2$ moving along the φ -axis within the so called tilted washboard potential field $-\left(\frac{\Phi_0 I_c}{2\pi}\right) \cos \varphi - \left(\frac{\Phi_0 I_0}{2\pi}\right) \varphi$. The Lagrangian and Hamiltonian of the junction was accordingly formulated, where it became clear that the conjugate variables of the system are the quantum phase difference across the junction φ and the

number of Cooper pairs stored in the junction's capacitance. Having the classical variables replaced by their corresponding quantum operators, the unbiased Josephson resonator was quantized whose anharmonicity was approximated by a quartic potential. The quartic term was treated as a perturbation to an SHO, and the eigenenergies and eigenstates of the perturbed system were calculated to the first order. It turned out that the deviation of the eigenenergies from those of an SHO quadratically increases for higher order states, and its sign is always negative indicating the fact that the actual potential is weaker than that of an SHO. Moreover, it was shown that the levels tend to become closer for higher order levels, which is consistent with the aforementioned fact that the potential of the Josephson resonator is softer than that of an SHO. The eigenstates of the system were expanded in terms of pure number states wherein the only nonzero terms are $|n\rangle$, $|n \pm 2\rangle$, and $|n \pm 4\rangle$. The variation of the expansion coefficients revealed the fact that although for a low n the perturbed state resembles $|n\rangle$, higher order states asymptotically approach to $(|n + 2\rangle - |n - 2\rangle)$.

Chapter 4

Macroscopic Tunneling and the Caldeira-Leggett Method

4.1 Introduction

Seeking quantum coherence in electrical circuits is conceptually initiated by Leggett in his pioneering discussion of macroscopic quantum phenomena, where a macroscopic quantum system was formally defined and proposals for their measurements as well as theoretical predictions about the results were presented [21–25].

At a fundamental level, the general belief that there is no “natural limit” for the realm of validity of quantum mechanics raises the “quantum measurement paradox”, which in its “most spectacular” form was stated by Schrödinger as the “cat paradox” [26], simply following the argument that quantum mechanics should describe the behavior of macroscopic bodies such as cats as well as atoms and electrons [27, 28].

In order to experimentally test this idea, we need to have a “macroscopic coordinate” X whose different values correspond to “macroscopically distinguishable” states of the

system. An immediate objection is that for a macroscopic system the energy level spacings are very tiny and are blurred out by thermal effect even at lowest temperatures and we shall not be able to observe any quantum effects in these levels. This objection is not correct; for example, if X is the flux through a simple LC circuit, the level spacing is $\hbar\omega_0$, where $\omega_0 \equiv 1/\sqrt{LC}$ is the resonant frequency of the circuit as shown in Chapter 1, and it is not difficult to make this spacing large compared to thermal energy at attainable temperatures [27].

As discussed in [28], the most promising phenomenon to look for is quantum tunneling because it fulfills the aforementioned requirement and is a purely quantum mechanical effect unlike discretization of the energy levels of an LC resonator which is right at the correspondence limit. A suitable system for observation of quantum tunneling should have the following properties. First, it has a metastable state that is separated from a more stable continuum of states by an energy barrier. Second, the points at which the system “enters” and “exits” from the barrier should correspond to macroscopically distinguishable states. Third, the frequency of small oscillations around the equilibrium position ω_0 should satisfy $\hbar\omega_0 \gg k_B T$ with attainable temperatures in order to distinguish transitions due to quantum tunneling from the ones due to thermal fluctuations. Fourth, the barrier should not be too large, otherwise the lifetime of metastable states would be unobservably long [27].

In particular, SQUIDS¹ [29] and current-biased single Josephson junctions [30] are two systems that fit very well to these conditions; the latter of which was discussed in Chapter 3, where its macroscopic conjugate variables, associated potential barrier, energy quantization, and tunneling out of the metastable states were identified.

In this chapter, we focus on the effect of dissipation on the macroscopic quantum tunneling within the Caldeira-Leggett framework which uses the instanton path integral

¹SQUID stands for Superconducting QUantum Interference Device.

methods. Given that the original Caldeira-Leggett work is very profound, general, and extensive, we are only at a position of utilizing a simplified version of their arguments and results which mostly concerns quantum mechanics of dissipation in selected cases. First, we will formulate the problem of tunneling from a metastable state for both lossless and dissipative systems, where in the latter case the parameters of the Lagrangian are related to the phenomenological damping coefficient. Different classes of dissipation are identified including the separable, linear, and strictly linear damping. The rate of escape from the metastable state are found in the WKB limit which involves an exponential form with the exponent being the dominant factor. Next, we will present the instanton method in order to calculate this exponent for both lossless and dissipative situations, where upper and lower bounds are found for the tunneling rate. It will be shown that the effect of dissipation is always to suppress the tunneling and in case of strictly linear damping is independent of the model. Then, the method is applied to a quadratic plus cubic potential, which coincides with the potential barrier of a driven Josephson anharmonic oscillator as discussed in the previous Chapter. Upper and lower bounds are calculated for the tunneling at intermediate damping, whereas approximate expressions are derived for the overdamped and underdamped limits. Finally, the dissipation-fluctuation theorem is verified for a damped simple harmonic oscillator, and the limits of high- and low-temperatures are examined.

4.2 Tunneling and Dissipation

A macroscopic system is inherently dissipative and has a complex interaction with its environment. A microscopic system which undergoes tunneling also interacts with environment but in most cases the interactions are sufficiently weak to be ignored or treated as small perturbations. But the dissipation in macroscopic tunneling systems may be very

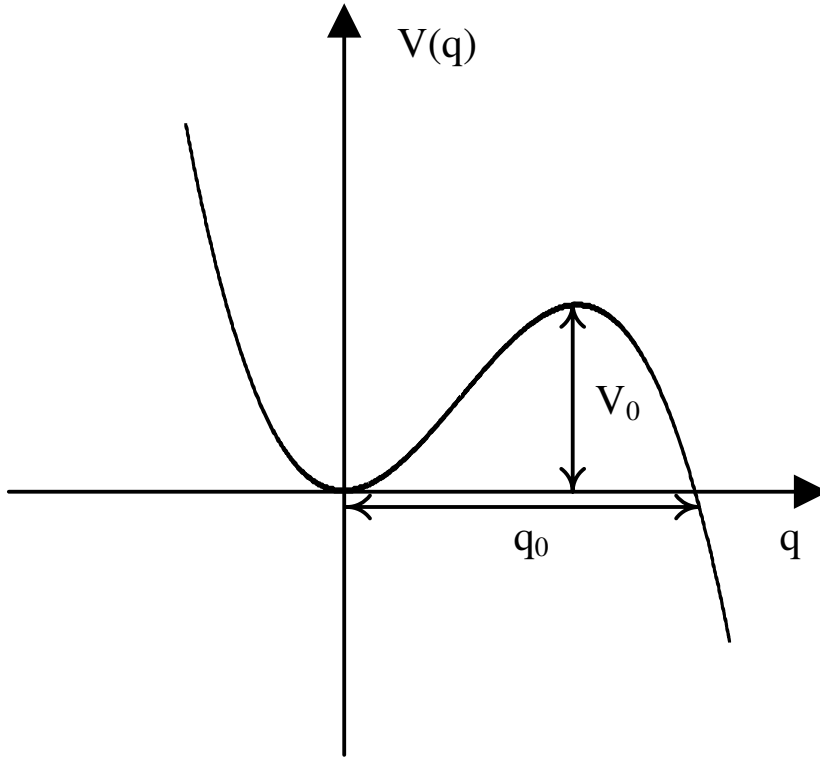


Figure 4.1: The form of the potential $V(q)$ considered in the subsequent calculations.

strong; for example a typical *rf*-SQUID may be overdamped. For microscopic systems with considerable coupling to the environment, there is usually a knowledge of the interaction Hamiltonian or of its principal features; in macroscopic systems, however, the dissipation mechanism is not of interest and its effect is described by phenomenological coefficients [27].

Consider a macroscopic system at zero temperature with a principal coordinate q subjected to a potential $V(q)$ with a metastable minimum at $q = 0$, which is chosen to be the zero of potential energy, as shown in Fig. 4.1. $V(q)$ also equals to zero at $q = q_0$, and is negative for $q > q_0$, i.e. beyond the potential barrier whose height is V_0 . The system

may leave the metastable quantum well by tunneling through the potential barrier; thus, $q = q_0$ is the “exit point” and the assumption that $V(q) < 0$ for $q > q_0$ will ensure that it will never return to the well. Note that q does not need to be a geometrical coordinate, however, for simplicity we assume that q is a geometrical coordinate and it is associated with a mass m . For example, for a SQUID q is the magnetic flux in the ring and m equals to the Josephson junction’s capacitance C , whereas for a biased Josephson junction q is the quantum phase difference across the junction ϕ and m is proportional to C as in (3.21). The following Lagrangian describes such a system:

$$\mathcal{L}(q, \dot{q}) = \frac{1}{2}m\dot{q}^2 - V(q), \quad (4.1)$$

with a classical equation of motion

$$m\ddot{q} + \frac{dV}{dq} = F_{ext}, \quad (4.2)$$

where F_{ext} is the external force. The frequency of oscillations around metastable minimum is given by

$$\omega_0 = \left(m^{-1} \frac{d^2V}{dq^2} \Big|_{q=0} \right)^{1/2}. \quad (4.3)$$

The WKB approximation is applicable to the tunneling behavior of the system, provided that the height of potential barrier is large compared to $\hbar\omega_0$. If the uncertainty $\Delta q = \langle (q - \langle q \rangle)^2 \rangle^{1/2}$ is small so that $q = \langle q \rangle$ and the potential $V(q)$ is slowly varying, one can write

$$\frac{d}{d\langle q \rangle} V(\langle q \rangle) = \left\langle \frac{d}{dq} V(q) \right\rangle, \quad (4.4)$$

and by employing the Ehrenfest's Theorem,

$$\frac{d}{dt}\langle p_q \rangle = -\langle \frac{\partial}{\partial q} V(q) \rangle, \quad (4.5)$$

we arrive at [31],

$$\frac{d}{dt}\langle p_q \rangle = -\frac{\partial}{\partial \langle q \rangle} V(\langle q \rangle). \quad (4.6)$$

Because of these assumptions, namely the shape of $V(q)$ and the fact that $V_0 \ll \hbar\omega_0$, (4.6) is approximately valid; therefore, we can conclude that the expectation value of coordinate q satisfies equation of motion (4.2). Using the WKB approximation we get

$$P_0 = A_0 \exp(-B_0/\hbar), \quad (4.7)$$

where P_0 is the probability of the escape of the system per unit time from the potential well when it is initially in the well. As seen from (4.7), the tunneling behavior of the system is dominated by the exponential factor B_0 . Now suppose that the system interacts with environment and this effect is incorporated in our equations through a phenomenological friction coefficient η , which must be obtained from experiment in any particular case. Thus the system's damped quasi-classical equation of motion is

$$m\ddot{q} + \eta\dot{q} + \frac{dV}{dq} = F_{ext}, \quad (4.8)$$

with the dissipated power per unit time equals to $\eta\dot{q}^2$. Here we need to make two more assumptions in order to proceed. First, any degree of freedom of the environment is weakly perturbed by the system. This way we can represent the environment as a bath of harmonic oscillators. Second, the system-bath coupling is linear in the oscillator coordinates and only

a function of system coordinate q ,

$$\sum_j F_j(q)x_j, \quad (4.9)$$

where x_j s are the environmental coordinates. Such cases are called quasi-linear dissipation, whereas if F_j is also linear in system coordinates q , i.e.

$$F_j(q) = C_j q, \quad (4.10)$$

the dissipation is referred to as strictly linear, and if we only have

$$F_j(q) = C_j f(q), \quad (4.11)$$

the dissipation is called separable.

Now we want to compare the tunneling characteristics of a system described by (4.8) and the isolated system (4.2) when they are subjected to the same potential and the same mass and study the effect of dissipation on tunneling probability P_0 .

The quantization of a dissipative system is a problem many people tried to solve in the past. There have been different approaches to this problem, such as time dependent Hamiltonian theory [32], non-linear Schrödinger equation [33], [34], or the complex Hamiltonian [35]. All of these methods have tried to describe the system by some kind of Schrödinger equation without addressing the environment explicitly and only been justified by producing the known damped harmonic oscillator results in the limit of weak damping. The generalization of these methods to other problems is not straightforward since their theoretical foundations are not clear. Therefore we need to have a physical description of environment explicitly. One way is to describe the environment action on the system by statistical methods [36]; the other way is to suppose that the system and the environment

form a close system, namely the *universe*, write the Lagrangian for the *universe*, solve it for the motion of the whole, and extract the properties of the system from this solution. Within the latter approach, dissipation is nothing but the energy transfer from the single degree of freedom of the system to the infinite degrees of freedom of the environment [27]. In practice, our knowledge of the environment is quite limited; however, supposing that any degree of freedom of environment is only weakly perturbed around its equilibrium state by the system, it can be presented, at $T = 0$, by a set of simple harmonic oscillators [37]. The neat twist is that the assumption that “any degree of freedom of environment is only weakly perturbed by the system” by no means implies that the interaction is weak from the system’s point of view which interacts with a very large number of degrees of freedom [27]; thereby, the method is compatible with strong damping. Therefore the Lagrangian of the environment is

$$\mathcal{L}_{osc} = \sum_j \left(\frac{1}{2} m_j \dot{x}_j^2 - \frac{1}{2} m_j \omega_j^2 x_j^2 \right), \quad (4.12)$$

where x_j s are the environment’s coordinates, and the interaction Lagrangian reads

$$\mathcal{L}_{int} = \sum_j F_j(q) x_j - \frac{1}{2} \frac{F_j^2(q)}{m_j \omega_j^2}, \quad (4.13)$$

where the first term represents the system-environment coupling and the second term ensures that the system cannot lower its potential energy below the uncoupled value. To see this, note that for a given q the minimum potential of the universe (system plus environment) is attained at $x_j = F_j(q)/(m_j \omega_j^2)$, and the second term in (4.13) keeps $V(q)$ intact at this limit. Collecting the three parts of Lagrangian; namely (4.1), (4.12), (4.13),

we get

$$\begin{aligned} \mathcal{L} = & \frac{1}{2}m\dot{q}^2 - V(q) + \frac{1}{2} \sum_j (m_j \dot{x}_j^2 - m_j \omega_j^2 x_j^2) \\ & - \sum_j F_j(q) x_j - \sum_j \frac{F_j^2(q)}{2m_j \omega_j^2}. \end{aligned} \quad (4.14)$$

For linear dissipation, where (4.10) applies, the Lagrangian (4.14) would take the form

$$\begin{aligned} \mathcal{L} = & \frac{1}{2}m\dot{q}^2 - V(q) + \frac{1}{2} \sum_j (m_j \dot{x}_j^2 - m_j \omega_j^2 x_j^2) \\ & - q \sum_j C_j x_j - q^2 \sum_j \frac{C_j^2}{2m_j \omega_j^2}. \end{aligned} \quad (4.15)$$

In some cases we might know the exact microscopic model of the environment, like the case of an ideal oxide-layer Josephson junction [38], so that the parameters are known to us; in most cases, however, only a phenomenological description of dissipation can be obtained from experiment and this parametric description of the environment still needs to be related to such quantities. For the quasi-linear dissipation, i.e. (4.9), we have [27]

$$\frac{\pi}{2} \sum_j \frac{1}{m_j \omega_j^2} \left(\frac{\partial F_j}{\partial q} \right)^2 \delta(\omega - \omega_j) = \eta(q) \quad \omega \ll \omega_c, \quad (4.16)$$

where ω_c is the frequency at which (4.8) begins to break down. For strictly linear dissipation, (4.10), we have [27]

$$J(\omega) = \frac{\pi}{2} \sum_j \frac{C_j^2}{m_j \omega_j^2} \delta(\omega - \omega_j), \quad (4.17a)$$

where

$$J(\omega) = \eta\omega. \quad (4.17b)$$

Equation (4.17b) also implies that the dissipation is frequency independent when it holds for all frequencies of interests.

A variant of the “instanton technique”, well-known in particle physics, has been applied to calculate the zero-temperature tunneling rate out of the metastable minimum. This method has been used by Leggett to solve the Lagrangian (4.15) for the tunneling exponent B [27]. Next, by integrating out the environment variables, this rate can be represented in the form of an integral which only involves the system variable $q(\tau)$. A generalization of the “instanton” method has been originally formulated in the context of classical thermodynamic metastability [39] and has been applied to the calculation of the decay of metastable states in the field theory [40, 41].

4.3 The Instanton Technique for Isolated Systems

Consider a one-dimensional system along the q coordinate whose Lagrangian reads

$$\mathcal{L}(q, \dot{q}) = \frac{1}{2}m\dot{q}^2 - V(q), \quad (4.18)$$

where the potential $V(q)$ has a metastable minimum as before at $q = 0$ that is the zero of potential energy. The density matrix of such a system is [42]

$$\rho(q_i, q_f; \beta) \equiv \sum_n \psi_n^*(q_i) \psi_n(q_f) \exp(-\beta E_n), \quad (4.19)$$

where $\beta = 1/k_B T$ is the Boltzmann factor, k_B is the Boltzmann constant, $\exp(-\beta E_n)$ is the probability of occupying a state with energy E_n for a system in thermal equilibrium at a temperature T , and q_i and q_f respectively are the initial and final coordinate values.

Using the path integral technique [41],

$$B = \int_{-\infty}^{\infty} L_E(q, \dot{q}) d\tau, \quad (4.20)$$

where B is the exponent in (4.7), and L_E is the Euclidean Lagrangian $L_E(q, \dot{q})$

$$\mathcal{L}_E(q, \dot{q}) = \frac{1}{2}m\dot{q}^2 + V(q). \quad (4.21)$$

4.4 The Instanton Technique for Damped Systems

Now we apply this technique on the a dissipative system by considering the *universe* whose density matrix reads

$$\rho(q_i, \{x_{\alpha i}\}; q_f, \{x_{\alpha f}\}; \beta) \equiv \sum_n \psi_n^*(q_i, \{x_{\alpha i}\}) \psi_n(q_f, \{x_{\alpha f}\}) \exp(-\beta E_n), \quad (4.22)$$

where q and x_α respectively refer to the system and environment coordinates, and i and f subscripts denote their final and initial values. The reduced density matrix of the system is

$$\begin{aligned} K(q_i, q_f; \beta) &\equiv \int \Pi_\alpha dx_{\alpha i} \rho(q_i, \{x_{\alpha i}\}; q_i, \{x_{\alpha i}\}; \beta) \\ &= \int \Pi_\alpha dx_{\alpha i} \sum_n \psi_n^*(q_i, \{x_{\alpha i}\}) \psi_n(q_f, \{x_{\alpha i}\}) \exp(-\beta E_n). \end{aligned} \quad (4.23)$$

Note that the environment coordinates have equal initial and final values, namely $\{x_{\alpha i}\}$, which reflects the assumption that any one degree of freedom of the environment is only weakly perturbed by the system. As in the non-dissipative case the tunneling rate P can

be written, in the *WKB* limit, in the form

$$P = A \exp(-B/\hbar), \quad (4.24)$$

where

$$B \equiv \int_{-\infty}^{\infty} \left\{ \frac{1}{2} m \dot{q}^2 + V(q) \right\} d\tau + \frac{1}{2} \int_{-\infty}^{\infty} d\tau' \int_{-\infty}^{\infty} d\tau \alpha(\tau - \tau') \{q(\tau) - q(\tau')\}^2, \quad (4.25)$$

and

$$\begin{aligned} \alpha(\tau - \tau') &\equiv \sum_j \frac{C_j^2}{4m_j \omega_j} \exp(-\omega_j |\tau - \tau'|) \\ &= \frac{1}{2\pi} \int_0^{\infty} J(\omega) \exp(-\omega |\tau - \tau'|) d\omega. \end{aligned} \quad (4.26)$$

We can also simplify α by the following approximation

$$\begin{aligned} \alpha(\tau - \tau') &= \frac{1}{2\pi} \int_0^{\infty} J(\omega) \exp(-\omega |\tau - \tau'|) d\omega \\ &\simeq \frac{1}{2\pi} \int_0^{\infty} \eta \omega \exp(-\omega |\tau - \tau'|) d\omega \\ &= \frac{\eta}{2\pi} \frac{1}{(\tau - \tau')^2} \end{aligned} \quad (4.27)$$

and then

$$B = \int_{-\infty}^{\infty} \left\{ \frac{1}{2} m \dot{q}^2 + V(q) \right\} d\tau + \frac{\eta}{4\pi} \int_{-\infty}^{\infty} d\tau' \int_{-\infty}^{\infty} d\tau \left\{ \frac{q(\tau) - q(\tau')}{(\tau - \tau')} \right\}^2. \quad (4.28)$$

This result has been obtained using the path-integral method for the Euclidean La-

grangian for the strictly linear damping

$$\begin{aligned}\mathcal{L} = & \frac{1}{2}m\dot{q}^2 + -V(q) + \frac{1}{2}\sum_j(m_j\dot{x}_j^2 + m_j\omega_j^2x_j^2) \\ & + q\sum_j C_jx_j + q^2\sum_j \frac{C_j^2}{2m_j\omega_j^2}.\end{aligned}\quad (4.29)$$

More generally, if we replace C_jq by $F(j)$ in (4.25), we get

$$B \equiv \int_{-\infty}^{\infty} \left\{ \frac{1}{2}m\dot{q}^2 + V(q) \right\} d\tau + \frac{1}{2} \int_{-\infty}^{\infty} d\tau' \int_{-\infty}^{\infty} d\tau \sum_j \frac{\exp(-\omega_j|\tau - \tau'|)}{4m_j\omega_j} \{F_j(q(\tau)) - F_j(q(\tau'))\}^2.\quad (4.30)$$

Having known that

$$\{F_j(q(\tau)) - F_j(q(\tau'))\}^2 = \left\{ \int_{q(\tau)}^{q(\tau')} \sqrt{\left(\frac{\partial F_j}{\partial q}\right)^2 dq} \right\}^2,\quad (4.31)$$

then,

$$\begin{aligned}& \sum_j \frac{\exp(-\omega_j|\tau - \tau'|)}{4m_j\omega_j} \{F_j(q(\tau)) - F_j(q(\tau'))\}^2 = \\ & \sum_j \frac{\exp(-\omega_j|\tau - \tau'|)}{4m_j\omega_j} \left\{ \int_{q(\tau)}^{q(\tau')} \sqrt{\left(\frac{\partial F_j}{\partial q}\right)^2 dq} \right\}^2 = \\ & \int_0^{\infty} \frac{\omega \exp(-\omega_j|\tau - \tau'|)}{2\pi} \sum_j \frac{\pi \delta(\omega - \omega_j)}{2 m_j\omega_j^2} \left\{ \int_{q(\tau)}^{q(\tau')} \sqrt{\left(\frac{\partial F_j}{\partial q}\right)^2 dq} \right\}^2 d\omega \leq \\ & \frac{1}{2\pi} \int_0^{\infty} \omega \exp(-\omega_j|\tau - \tau'|) \left\{ \int_{q(\tau)}^{q(\tau')} \sqrt{\eta(q)} dq \right\}^2 d\omega,\end{aligned}$$

where the equation (4.16) and the following inequality have been employed to carry out

the last step:

$$\sum_j \left\{ \int_{q(\tau)}^{q(\tau')} \sqrt{\left(\frac{\partial F_j}{\partial q}\right)^2} dq \right\}^2 \leq \left\{ \int_{q(\tau)}^{q(\tau')} \sqrt{\sum_j \left(\frac{\partial F_j}{\partial q}\right)^2} dq \right\}^2. \quad (4.32)$$

Using

$$\int_0^\infty \omega \exp(-\omega|\tau - \tau'|) d\omega = \frac{1}{(\tau - \tau')^2}, \quad (4.33)$$

we get

$$\frac{1}{2\pi} \int_0^\infty \omega \exp(-\omega|\tau - \tau'|) \left\{ \int_{q(\tau)}^{q(\tau')} \sqrt{\eta(q)} dq \right\}^2 d\omega = \frac{1}{2\pi(\tau - \tau')^2} \left\{ \int_{q(\tau)}^{q(\tau')} \sqrt{\eta q} dq \right\}^2. \quad (4.34)$$

Therefore,

$$B \leq \int_{-\infty}^\infty \left\{ \frac{1}{2} m \dot{q}^2 + V(q) \right\} d\tau + \frac{1}{2} \int_{-\infty}^\infty d\tau' \int_{-\infty}^\infty d\tau \frac{\left\{ \int_{q(\tau)}^{q(\tau')} \sqrt{\eta(q)} dq \right\}^2}{2\pi(\tau - \tau')^2}, \quad (4.35)$$

and we have found an upper limit for the effect of dissipation on tunneling. On the other hand, if the interaction is separable, i.e. (4.11) holds, then

$$\sum_j C_j^2 \left\{ \int_{q(\tau)}^{q(\tau')} \sqrt{\left(\frac{\partial f}{\partial q}\right)^2} dq \right\}^2 = \left\{ \int_{q(\tau)}^{q(\tau')} \sqrt{\sum_j C_j^2 \left(\frac{\partial f}{\partial q}\right)^2} dq \right\}^2; \quad (4.36)$$

hence, in (4.32), and consequently in equation (4.35), equality sign becomes valid and the exact expression for tunneling can be obtained.

In case of strictly linear dissipation (4.10), or equivalently $\eta(q) = \eta$, the equation (4.35) can be simplified into (4.28).

Since α in (4.26) is positive definite, the contribution of the last term in (4.28) is always

positive; therefore, in the WKB limit, the existence of dissipation always tends to suppress tunneling, and this result is independent of the form of the spectral density $J(\omega)$ [27]. The suppression of tunneling by dissipation is, in fact, a more general result as can be seen from (4.35). We can also see from (4.28) that the tunneling probability is only a function of friction coefficient η , and, therefore, the effect of dissipation on tunneling is uniquely determined by this single parameter for a given potential $V(q)$ and is not model-dependent. Although it has to be emphasized that this property is peculiar to the strictly linear case [27].

4.5 Quadratic Plus Cubic Potential

Consider a typical quadratic plus cubic potential like the one shown in Fig. 4.1,

$$V(q) = \frac{1}{2}m\omega_0^2q^2 - \beta q^3 = \frac{27}{4}V_0 \left\{ \left(\frac{q}{q_0}\right)^2 - \left(\frac{q}{q_0}\right)^3 \right\} \quad (4.37)$$

where

$$V_0 = \frac{m^3\omega_0^6}{54\beta^2}, \quad (4.38a)$$

$$q_0 = \frac{1}{2}m\omega_0\omega_0^2/\beta, \quad (4.38b)$$

and q_0 is the coordinate of the exit point. WKB results for quadratic plus cubic potential in the absence of dissipation, i.e. where the Lagrangian (4.1) describes the system, are [43]

$$P_0 = A_0 \exp(-B_0/\hbar), \quad (4.39a)$$

and

$$B_0 = \frac{36}{5} \frac{V_0}{\omega_0} = \frac{2}{15} \frac{m^3\omega_0^5}{\beta^2}. \quad (4.39b)$$

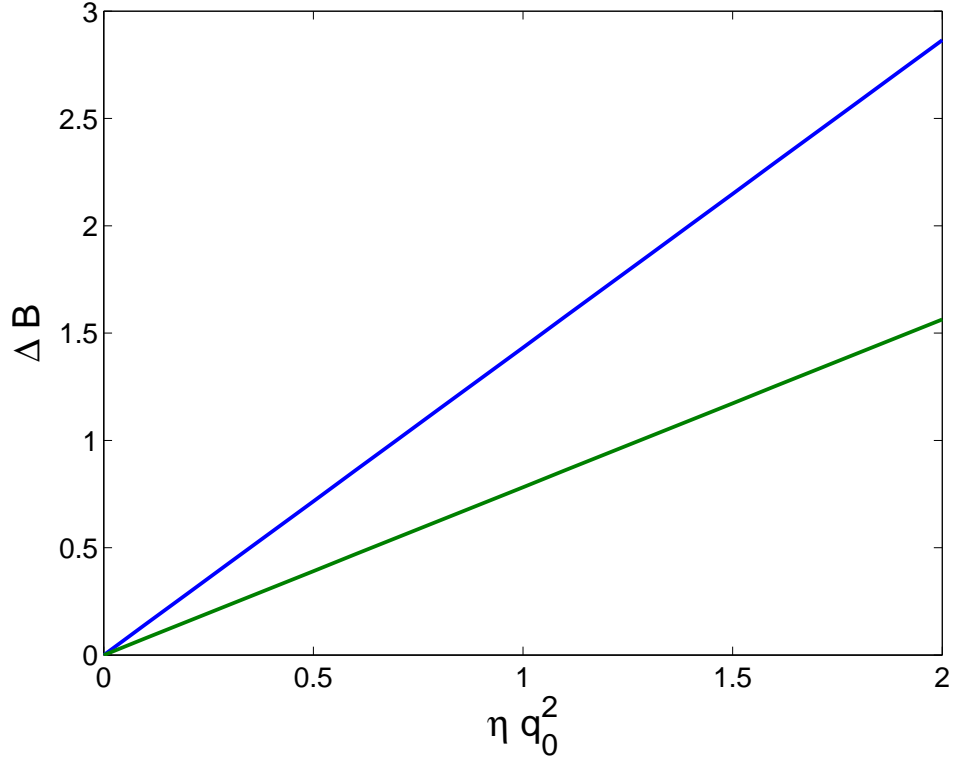


Figure 4.2: The lower and upper limits of the change in the exponent of tunneling probability in the case of quadratic plus cubic potential

For the strictly linearly damped system described by Lagrangian (4.15), we can use the method of the previous section to evaluate the exponent of (4.7) [27]. If we define for (4.28) [44],

$$B_0 = \int_{-\infty}^{\infty} \left\{ \frac{1}{2} m \dot{q}^2 + V(q) \right\} d\tau, \quad (4.40)$$

and

$$\Delta B = \frac{\eta}{4\pi} \int_{-\infty}^{\infty} d\tau' \int_{-\infty}^{\infty} d\tau \left\{ \frac{q(\tau) - q(\tau')}{(\tau - \tau')} \right\}^2, \quad (4.41)$$

the results can be summarized in the limit of strong and weak damping:

$$\Delta B = 12\zeta(3)/\pi^3 \quad \eta \longrightarrow 0, \quad (4.42a)$$

$$\Delta B = 2\pi/9 \quad \eta \longrightarrow \infty, \quad (4.42b)$$

and for intermediate situations

$$\frac{2\pi}{9}\eta q_0^2 \leq \Delta B \leq \frac{56\pi}{225}\eta q_0^2, \quad (4.43)$$

as shown in Fig. 4.2. Note that although ΔB becomes closer to its lower limit in strong damping, nevertheless it is an increasing function of ηq_0 .

4.6 Lagrangian of a Damped LC Resonator

In this section, we will show that the Lagrangian of a damped LC resonator can be written in the form of (4.15). For a simple LC circuit, if we choose the flux Φ to be the basic coordinate, the following Lagrangian describes the behavior of the circuit, as shown in Chapter 1:

$$\mathcal{L}(\Phi, \dot{\Phi}) = \frac{1}{2}C\dot{\Phi}^2 - \frac{1}{2L}\Phi^2. \quad (4.44)$$

When a normal resistor is connected to the circuit in parallel to the capacitor, the correction to the Lagrangian would be

$$\Delta\mathcal{L} = I_n\Phi, \quad (4.45)$$

where I_n is the current flowing through the resistor $I_n = -\sigma_n \dot{\Phi}$, and σ_n is the normal conductance of the resistor [27]. Therefore,

$$\mathcal{L}(\Phi, \dot{\Phi}) = \frac{1}{2}C\dot{\Phi}^2 - \frac{1}{2L}\Phi^2 + I_n\Phi. \quad (4.46)$$

Since

$$Q_n = \int_0^t I_n(t')dt', \quad (4.47)$$

one may rewrite Q_n in terms of the normal coordinates of the resistor Q_α

$$Q_n = \sum_j \tilde{C}_j Q_j, \quad (4.48)$$

thus

$$\Delta\mathcal{L} = \Phi \sum_j \tilde{C}_j \dot{Q}_j. \quad (4.49)$$

With the following change of coordinates

$$x_j = \omega_j^{-1}(\dot{Q}_j + \tilde{C}_j\Phi/m_j), \quad (4.50)$$

the Lagrangian reads

$$\begin{aligned} \mathcal{L} = & \frac{1}{2}C\dot{\Phi}^2 - \frac{\Phi^2}{2L} + \frac{1}{2} \sum_j (m_j \dot{x}_j^2 - m_j \omega_j^2 x_j^2) \\ & - \Phi \sum_j C_j x_j - \Phi^2 \sum_j \frac{C_j^2}{2m_j \omega_j^2}, \end{aligned} \quad (4.51)$$

which casts into the form of (4.15), where $c_j \equiv \omega_j \tilde{C}_j$ and

$$J(\omega) = \frac{\pi}{2} \sum_j \frac{C_j^2}{m_j \omega_j^2} \delta(\omega - \omega_j) = \sigma_n \omega. \quad (4.52)$$

4.7 Damped Harmonic Oscillator

In this section, we will use a Lagrangian of the form (4.15) for a damped harmonic oscillator, and treat the problem using the instanton method. A damped harmonic oscillator obeys the Lagrangian in 4.15 with $V(q) = \frac{1}{2} M \omega_0^2 q^2$, i.e.

$$\begin{aligned} \mathcal{L} = & \frac{1}{2} m \dot{q}^2 - \frac{1}{2} m \omega_0^2 q^2 + \frac{1}{2} \sum_j (m_j \dot{x}_j^2 - m_j \omega_j^2 x_j^2) \\ & - q \sum_j C_j x_j - q^2 \sum_j \frac{C_j^2}{2m_j \omega_j^2}. \end{aligned} \quad (4.53)$$

The density matrix of such a system reads

$$K(X, \zeta; \beta) = \text{const} \exp\left(-\frac{1}{2} \{\lambda^{-1} X^2 + \mu \zeta^2\}\right), \quad (4.54)$$

where $X = (q_i + q_f)/2$ and $\zeta = q_i - q_f$ are center of mass and relative variables, with

$$\lambda = \frac{\hbar}{m} \sum_n \frac{1}{\omega_n^2 + \omega_0^2 + 2\gamma|\omega_n|}, \quad (4.55a)$$

and

$$\mu = \frac{m\beta^{-1}}{\hbar} \sum_n \left(1 - \frac{1}{\omega_n^2 + \omega_0^2 + 2\gamma|\omega_n|}\right), \quad (4.55b)$$

where $\gamma \equiv \eta/2m$. Moreover,

$$\langle q^2 \rangle = \int X^2 K(X, 0; \beta) dX = \lambda, \quad (4.56a)$$

and

$$\langle p^2 \rangle = \int dX \int dp p^2 \int \exp(ip\zeta/\hbar) K(X, \zeta; \beta) dX = \hbar^2 \mu. \quad (4.56b)$$

For example, consider the circuit configurations shown in Fig. 4.3. For the undamped resonator with the Lagrangian (4.44) the fluctuations of flux and charge are

$$\langle \Phi^2 \rangle = \frac{\hbar}{2C\omega_0}, \quad \text{and} \quad \langle Q^2 \rangle = \frac{1}{2}\hbar\omega_0 C. \quad (4.57)$$

Now, if we add a resistor in parallel with the capacitor then the coordinate variable is Φ with the equation of motion

$$C\ddot{\Phi} + R^{-1}\dot{\Phi} + L^{-1}\Phi = I_{ext}, \quad (4.58)$$

and the corresponding momentum is $-Q$. The dissipation in this case is proportional to $R^{-1}\dot{\Phi}^2$. Therefore, according to (4.55) and (4.56), the presence of dissipation will decrease the mean square fluctuation of $\langle \Phi^2 \rangle$ relative to its value (4.57) and increases the mean square fluctuations of $\langle Q^2 \rangle$. However if the resistor is added in series with the inductor, then the coordinate variable is Q with the equation of motion

$$L\ddot{Q} + R\dot{Q} + C^{-1}Q = V_{ext}, \quad (4.59)$$

and the corresponding momentum is Φ . The dissipation in this case is proportional to $R\dot{Q}^2$. In this case the presence of dissipation will increase the mean square fluctuation of

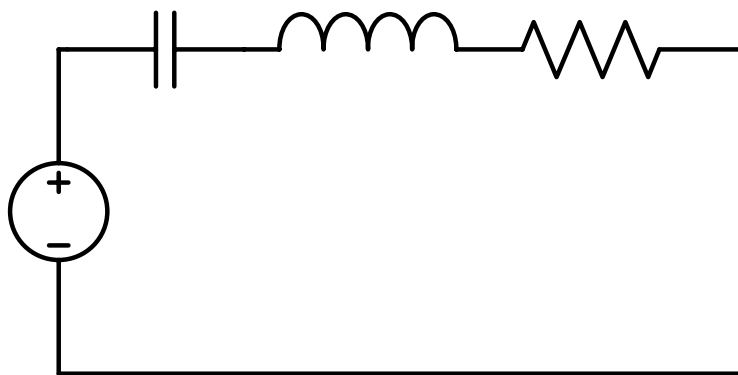
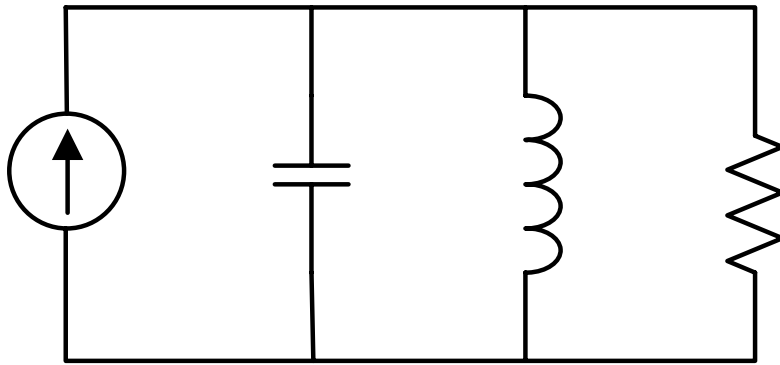
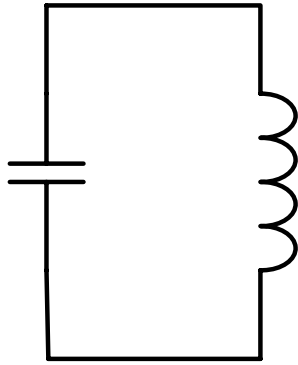


Figure 4.3: Circuit Configurations

$\langle \Phi^2 \rangle$ relative to its value (4.57) and decreases the mean square fluctuations of $\langle Q^2 \rangle$. [45]

4.8 The High- and Low-Temperature Limits

Using Kramers-Kronig and longitudinal sum rules [46] we see that in high temperatures the asymptotic behavior of $\langle q^2 \rangle$ and $\langle p^2 \rangle$ is [27]

$$\lambda \longrightarrow (\beta m \omega_0^2)^{-1}, \quad (4.60)$$

and

$$\mu \longrightarrow \left(\frac{m}{\hbar^2 \beta} \right), \quad (4.61)$$

thus,

$$K(X, \zeta; \beta) = \text{const} \exp \left\{ -\frac{1}{2} \left[(\beta m \omega_0^2) X^2 + \left(\frac{m}{\hbar^2 \beta} \right) \zeta^2 \right] \right\}. \quad (4.62)$$

At the zero temperature limit

$$\lambda = \frac{\hbar}{2m\omega_0} f(\alpha) \quad \text{and} \quad \alpha = \frac{\gamma}{2\omega_0}, \quad (4.63)$$

where

$$f(\alpha) = \frac{1}{\sqrt{1-\alpha^2}} \left[1 - \frac{2}{\pi} \tan^{-1} \frac{\alpha}{\sqrt{1-\alpha^2}} \right] \quad \alpha \leq 1, \quad (4.64a)$$

$$f(\alpha) = \frac{1}{\sqrt{\alpha^2-1}} \frac{1}{\pi} \left[\ln \frac{\alpha + \sqrt{\alpha^2-1}}{\alpha - \sqrt{\alpha^2-1}} \right] \quad \alpha \geq 1, \quad (4.64b)$$

$$f(\alpha) = \frac{2}{\pi} \quad \alpha = 1, \quad (4.64c)$$

$$f(\alpha) = \frac{2}{\pi \alpha} \ln(2\alpha) \quad \alpha \gg 1. \quad (4.64d)$$

We can see from the last expression that the probability density distribution in the overdamped limit is narrowed for oscillator coordinate and broadened for the momentum [27].

4.9 Summary and Discussion

This chapter discussed the effects of dissipation on quantum tunneling based on elegant work of Caldeira and Leggett. The problem of quantum tunneling from a metastable state to a continuum was formally formulated for lossless and dissipative cases, where proper Lagrangian was derived for both cases. For the dissipative tunneling, the parameters of the Lagrangian were related to the phenomenological dissipation coefficient in the classical equation of motion of the system, where different classes of dissipation were identified including quasi-linear, strictly linear, and separable dissipations. It was shown that in the WKB limit the rate of escape from the metastable quantum well is an exponential function depending to the height of the barrier. The instanton method, in turn, was employed to find the exponent in both the lossless and dissipative tunneling. Upper and lower bounds were found for the deviation of the tunneling exponent from the lossless case. It was demonstrated that dissipation, in general, suppresses the tunneling, and for the case of strictly linear dissipation it can be determined from the single phenomenological loss coefficient and is independent of the model. The method then was applied to a quadratic plus cubic potential, which is the potential field of a current biased Josephson resonator as shown in the previous chapter. An inequality for the deviation of the tunneling exponent was found for intermediate dissipation, whereas at the overdamped and underdamped limits approximate expression were derived. It was shown that although this deviation approaches to the lower limit for strong damping, it is an increasing function of ηq_0 , where η is the phenomenological loss coefficient and q_0 is the width of the potential barrier.

Moreover, the special form of the Lagrangian which envisions the dissipation mechanism as transfer of energy from the one degree of freedom of the system to the infinite degrees of freedom of the environment is justified for a lossy LC circuit. Based on this Lagrangian, the dissipation-fluctuation was verified for a damped harmonic oscillator without imposing the condition of weak damping. It was shown that for a parallel LC resonator where the magnetic flux is taken as the coordinate variable, dissipation decreases the fluctuations in Φ , whereas the fluctuations in its conjugate variable Q is increased. For a series LC resonator, on the other hand, where Q is the coordinate variable the fluctuations in Φ is increased and in Q is reduces. Finally, the asymptotic behavior of the uncertainty relations for the coordinate and conjugate variables were addressed at the high- and low-temperature limits.

Chapter 5

Concluding Remarks

This thesis has investigated the quantum mechanical behavior of electric circuits including LC resonators, finite length terminated microwave transmission line resonators, and Josephson junction resonators.

In chapter 1, the classical Lagrangian and Hamiltonian of LC resonator system were constructed based on the correspondence of electric and magnetic energies to kinetic and potential energies. The magnetic flux Φ was chosen as the independent variable q , so the electric charge Q turned out to be the canonical conjugate momentum p . While the system represented an electromagnetic simple harmonic oscillator (SHO) with a mass C and a resonance frequency $\omega_o = 1/\sqrt{LC}$, second quantization was applied to obtain the quantum Hamiltonian operator, which, in turn, was diagonalized using the annihilation and creation operators. The averages and uncertainties of flux, charge, current, and voltage were obtained for the number states $|n\rangle$ as well as the coherent states $|\alpha\rangle$. It was demonstrated while maintaining the resonance frequency unchanged, increasing the capacitance C reduces the uncertainties in the flux and voltage at the expense of increasing the uncertainties of the charge and current. The density matrix of the LC resonator was introduced

and its time evolution starting from a coherent state $|\alpha_0\rangle$ was studied, for both lossless and dissipative cases, based on a quantum optical treatment utilizing the P-representation of the density operator. In case of a lossless resonator the state of the circuit only underwent a phase change. For RLC resonator, where the loss was modeled by means of coupling to a bath of SHOs, a Fokker-Plank equation was obtained for the P-representation. It was shown that the P-representation starting from a delta function moves down an exponential spiral towards the vacuum state, and suffers from damping and broadening over the time. While the averages of the flux and charge, or equivalently current and voltage, undergo exponentially damped oscillations toward zero, for the RLC resonator, the uncertainty product $\Delta\hat{\Phi} \cdot \Delta\hat{Q}$ increases over time and asymptotically reaches its final value, which clearly manifests acquisition of noise by the lossy resonator.

Chapter 2 studied microwave resonators realized by a finite transmission line terminated at both ends by loads of unity magnitude reflection coefficients. This last condition was shown to be essential for realizing a lossless microwave resonator; otherwise imperfect reflections from the loads would dissipate the energy of the resonator, even though the comprising transmission line being lossless. While an LC circuit is a zero dimensional structure, a transmission line is a one dimensional structure comprised of an infinite number of infinitesimal LC resonators. Therefore, the correspondence between electric and magnetic energies to kinetic and potential energies was used once again to obtain the Lagrangian at a single point along the transmission line wherein the magnetic flux $\Phi(z, t)$ threading the cross section of the transmission line was taken as the independent variable and the electric charge $Q(z, t)$ found as the canonical conjugate momentum. The canonical coordinate and momentum were expanded in terms of the standing wave Fourier series, as the normal collective modes of the system. The resulting Hamiltonian represented an infinite number of discrete spectrum SHOs corresponding to different resonance modes of the cavity. Second

quantization was accordingly applied, and the Hamiltonian operator was diagonalized by means of ladder operators a_n^\dagger and a_n associated with each mode. The averages and uncertainty relations were found for both lossless and dissipative modes, wherein the latter case the same quantum optical approach of chapter 1 was employed. It was shown that increasing/decreasing the characteristic impedance of the line, while maintaining the resonance frequency unchanged, will reduce/increase the uncertainty of the flux/charge operators. In addition, the uncertainty product was shown to be higher for higher order modes. The effect of the length and terminations on the spectrum of the resonator and the uncertainty relations are explicitly demonstrated through the dependence of the resonance frequency of the system on the phase of reflection coefficients.

Chapter 3 studied the Josephson anharmonic oscillator. The intrinsic nonlinearity of a Josephson junction was exploited to investigate an anharmonic system where the energy separation between adjacent levels are not equal. It was shown that the Josephson resonator resembles a mass of $C \left(\frac{\Phi_0}{2\pi}\right)^2$ moving in a tilted washboard potential. The stationary states of an unbiased Josephson resonator were found by means of approximating the potential as a quadratic plus quartic form and applying the perturbation method. It was shown that the energy separation between adjacent levels is less than $\hbar\omega$ since the potential is weaker than a harmonic potential. The fidelity of the eigenstates was also studied and it was found that while low order levels closely resemble pure number states $|n\rangle$, higher order levels approach to the superposition of $|n-2\rangle$ and $|n+2\rangle$. For biased Josephson resonator, the potential was approximated as a quadratic plus cubic form, and the possibility of the resonator escaping from the metastable states of the quantum well by means of tunneling was highlighted.

In chapter 4, the problem of macroscopic quantum tunneling in the presence of dissipation was reviewed based on the Caldeira-Leggett method. The instanton technique was

briefly addressed for both lossless and dissipative systems. It was shown that this method gives the correct result for the known case of damped harmonic oscillator. Moreover, the effect of dissipation on the fluctuations in both series and parallel RLC circuits was examined. The method was also applied to the case of quadratic plus cubic potential. While this case represents tunneling from zero-voltage states of a driven Josephson resonator into voltage states, approximate expressions for the tunneling rate was derived for the underdamped and overdamped cases at the WKB limit, and upper and lower bounds was found for the case of intermediate dissipation. The limits of high and low temperatures were addressed accordingly.

Bibliography

- [1] C. A. Desoer and E. S. Kuh, *Linear and Nonlinear Circuits*. New York: McGraw-Hill, 1987.
- [2] A. Yariv, *Quantum Eletronics, 3rd Ed.* New York: John Wiley & Sons, 1989.
- [3] K. K. Clarke and D. T. Hess, *Commucication Circuits: Analysis and Design*. Massachusetts: Addison-Wesley, 1971.
- [4] D. M. Pozar, *Microwave Engineering*. New York: John Wiley & Sons, 1998.
- [5] W. H. Louisell, *Quanatam Statistical Properites of Radiation*. New York: John Wiley & Sons, 1973.
- [6] H. Goldstein, C.Poole, and J. Safko, *Classical Mechnics, 3rd Ed.* New York: Addison-Wesley, 2000.
- [7] B. L. Moiseiwitsch, *Variational Principles*. London: Wiley, 1966.
- [8] R. Shankar, *Principles of Quantum Mechanics, 2nd Ed.* New York: Kluwer Academics, 1994.
- [9] M. O. Scully and M. S. Zubairy, *Quantum Optics*. Cambridge: Cambridge University Press, 1997.

- [10] J. Clarke, A. N. Cleland, M. H. Devoret, D. Esteve, and J. M. Martinis, “Quantum mechanics of a macroscopic variable: The phase difference of a josephson junction,” *Science*, vol. 239, pp. 992–997, 1988.
- [11] L. I. Schiff, *Quantum Mechanics, 2nd Ed.* New York: McGraw-Hill, 1955.
- [12] R. E. Collin, *Field Theory of Guided Waves.* New York: McGraw-Hill, 1960.
- [13] P. Yeh, *Optical Waves in Layered Media.* New York: John Wiley & Sons, 2005.
- [14] J. Clarke and F. K. Wilhelm, “Superconducting quantum bits,” *Science*, vol. 453, pp. 1038–1042, 2008.
- [15] A. Barone and G. Paterno, *Physics and Applications of the Josephson Effect.* New York: John Wiley & Sons, 1982.
- [16] J. Bardeen, L. N. Cooper, and J. R. Schrieffer, “Theory of superconductivity,” *Phys. Rev. B*, vol. 108, pp. 1175–1204, 1957.
- [17] J. E. Mercereau, “Macroscopic quantum phenomena,” in *Superconductivity, Vol. 1*, R. D. Park, Ed. New York: Marcel Dekker, 1969.
- [18] T. Orlando and K. A. Delin, *Foundations of Applied Superconductivity.* Massachusetts: Addison-Wesley, 1991.
- [19] L. Yu, N. Newman, J. Rowell, and T. Van Duzer, “Incorporation of a frequency-dependent dielectric response for the barrier material in the josephson junction circuit model,” *IEEE Trans. Appl. Supercond.*, vol. 15, pp. 3886–3900, 2005.
- [20] H. Xu, A. J. Berkley, A. M. Gubrud, R. C. Ramos, J. R. Anderson, C. J. Lobb, and F. C. Wellstood, “Analysis of energy level quantization and tunneling from the zero-

- voltage state of a current-biased josephson junction,” *IEEE Trans. Appl. Supercond.*, vol. 13, pp. 956–3900, 2003.
- [21] A. J. Leggett, “Macroscopic quantum tunneling and related effects in josephson systems,” in *Percolation, Localization, and Supperconductivity*, A. M. Goldman and S. A. Wolf, Eds. New York: Plenum Press, 1984.
- [22] —, “Quantum mechanics at the macroscopic level,” in *Chance and MAtter*, J. V. J. Souletie and R. Stora, Eds. Netherlands: North Holland, 1987.
- [23] —, “Quantum mechanics at the macroscopic level,” in *Directions in Condensed Matter Physics*, G. Grinstein and G. Mazenko, Eds. Philadelphia, PA, USA: World Scientific Pub, 1986.
- [24] —, “Reflections on the quantum measurement paradox,” in *Quantum Implications: Essays in Honour of David Bohm*, F. D. P. B. J. Hiley, Ed. New York: Routledge and Kegan Paul, 1987.
- [25] —, “Macroscopic quantum tunnelling and all that,” in *Essays in Theoretical Physics: In Honour of Dirk Ter Haar*, W. E. Parry, Ed. London: Pergamon, 1984.
- [26] E. Schrödinger, “The present situation in quantum mechanics,” *Die Naturwissenschaften*, vol. 23, p. 807, 1935.
- [27] A. O. Caldeira and A. J. Leggett, “Quantum tunnelling in a dissipative system,” *Ann. Phys.*, vol. 149, pp. 374–456, 1983.
- [28] A. J. Leggett, “Macroscopic quantum systems and the quantum theory of measurement,” *Prog. Theor. Phys. Supplement*, vol. 69, p. 80, 1980.

- [29] O. V. Lounasmaa, *Experimental Principles and Methods Below 1K*. New York: Academic Press, 1974.
- [30] M. Ivanchenko and L. A. Zilberman, *PZh. Eksp. Teor. Fiz.*, vol. 55, pp. 2393[Sov. Phys.JETP. 28, 1272 (1969)], 1968.
- [31] A. F. J. Levi, *Applied Quantum Mechanics, 2nd Ed.* Cambridge: Cambridge University Press, 2006.
- [32] E. Kanai, “On the quantization of the dissipative systems,” *Prog. Theor. Phys.*, vol. 3, pp. 440–442, 1948.
- [33] M. D. Kostin, “Schrödinger-Langevin equation,” *J. Chem. Phys.*, vol. 57, p. 3589, 1972.
- [34] K. Yasue, “Quantum-mechanics of non- conservative systems,” *Ann. Phys.*, vol. 114, p. 479, 1978.
- [35] H. Dekker, “Quantization of linearly damped harmonic-oscillator,” *Phys. Rev. A*, vol. 16, pp. 2126–2134, 1977.
- [36] R. H. Koch, D. J. V. Harlingen, and J. Clarke, “Quantum-noise theory for the resistively shunted josephson junction,” *Phys. Rev. Lett.*, vol. 45, p. 2132, 1980.
- [37] K. Möhring and U. Smilansky, “A semi-classical treatment of dissipative processes based on feynman’s influence functional method,” *Nucl. Phys. A*, vol. 338, pp. 227–268, 1980.
- [38] V. Ambegaokar, U. Eckern, and G. Schön, “Quantum dynamics of tunneling between superconductors,” *Phys. Rev. Lett.*, vol. 48, p. 1745, 1982.

- [39] J. S. Langer, “Theory of condensation point,” *Ann. Phys.*, vol. 41, p. 108, 1967.
- [40] M. Stone, “Semiclassical methods for unstable states,” *Phys. Lett. B*, vol. 67, p. 186, 1977.
- [41] C. G. Callan and S. Coleman, “Fate of the false vacuum. ii. first quantum corrections,” *Phys. Rev. D*, vol. 16, p. 1762, 1977.
- [42] R. P. Feynman and A. R. Hibbs, *Quantum Mechanics and Path Integrals*. New York: McGraw-Hill, 1965.
- [43] A. O. Caldeira, *Ph.D. Thesis*. unpublished: University of Sussex, 1980.
- [44] A. O. Caldeira and A. J. Leggett, “Influence of dissipation on quantum tunneling in macroscopic systems,” *Phys. Rev. Lett.*, vol. 46, p. 211, 1981.
- [45] A. J. Leggett, “Quantum tunneling in the presence of an arbitrary linear dissipation mechanism,” *Phys. Rev. B*, vol. 30, p. 1208, 1984.
- [46] D. Pines and P. Nozières, *The Theory of Quantum Liquids*. New York: Benjamin, 1966.
- [47] U. Leonhardt, *Measuring the Quantum State of Light*. Cambridge: Cambridge University Press, 1997.

Appendices

Appendix A

Single Harmonic Oscillator

The Hamiltonian of an object of a mass m oscillating in a quadratic potential field with an angular frequency of ω_0 is

$$H = \frac{\hat{p}^2}{2m} + \frac{1}{2}m\omega_0^2\hat{q}^2, \quad (\text{A.1})$$

where \hat{q} and \hat{p} respectively are the position and momentum operators satisfying the commutation relation

$$[\hat{p}, \hat{q}] = i\hbar. \quad (\text{A.2})$$

The Hamiltonian can be cast into a diagonal form by introducing the creation and annihilation operators [8]

$$a = \left(\frac{m\omega_0}{2\hbar}\right)^{1/2} \hat{q} + i \left(\frac{1}{2m\hbar\omega_0}\right)^{1/2} \hat{p}, \quad (\text{A.3a})$$

and

$$a^\dagger = \left(\frac{m\omega_0}{2\hbar}\right)^{1/2} \hat{q} - i \left(\frac{1}{2m\hbar\omega_0}\right)^{1/2} \hat{p}. \quad (\text{A.3b})$$

Obviously

$$\hat{q} = \left(\frac{\hbar}{2m\omega_0}\right)^{1/2} (a^\dagger + a), \quad (\text{A.4a})$$

and

$$\hat{p} = i \left(\frac{m\omega_0\hbar}{2} \right)^{1/2} (a^\dagger - a). \quad (\text{A.4b})$$

Clearly, the following commutation holds between a and a^\dagger

$$[a, a^\dagger] = 1. \quad (\text{A.5})$$

The diagonalized Hamiltonian, therefore, reads

$$H = \hbar\omega_0 \left(a^\dagger a + \frac{1}{2} \right). \quad (\text{A.6})$$

The state of the harmonic oscillator can be expanded as a superposition of number states $|n\rangle$, which follow

$$a^\dagger |n\rangle = \sqrt{n+1} |n+1\rangle, \quad (\text{A.7a})$$

$$a |n\rangle = \sqrt{n} |n-1\rangle, \quad (\text{A.7b})$$

$$H |n\rangle = \left(n + \frac{1}{2} \right) \hbar\omega_0 |n\rangle. \quad (\text{A.7c})$$

The following relations hold for the averages and uncertainties of the number states

$$\langle \hat{q} \rangle = 0, \quad (\text{A.8a})$$

$$\langle \hat{p} \rangle = 0, \quad (\text{A.8b})$$

$$\langle \hat{q}^2 \rangle = \frac{\hbar}{m\omega_0} \left(n + \frac{1}{2} \right), \quad (\text{A.8c})$$

$$\langle \hat{p}^2 \rangle = m\omega_0\hbar \left(n + \frac{1}{2} \right), \quad (\text{A.8d})$$

$$\Delta \hat{q} \cdot \Delta \hat{p} = \hbar \left(n + \frac{1}{2} \right). \quad (\text{A.8e})$$

Appendix B

Coherent States

Coherent states are the most classical-like states; they are the eigenstates of annihilation operator a . Since a is not a hermitian operator, the eigenvalues are not real. Moreover, the coherent states are not orthogonal or form a complete set. In order to find these eigenvectors we should solve the following eigenvalue problem [9, 47]

$$a|\alpha\rangle = \alpha|\alpha\rangle, \tag{B.1a}$$

$$\langle\alpha|a^\dagger = \langle\alpha|\alpha^*, \tag{B.1b}$$

where $\alpha = |\alpha|e^{i\theta}$ and $\theta = \text{real}$, which yields

$$|\alpha\rangle = e^{-\frac{1}{2}|\alpha|^2} \sum_{n=0}^{\infty} \frac{\alpha^n}{\sqrt{n!}} |n\rangle, \tag{B.2}$$

or alternatively

$$|\alpha\rangle = e^{-\frac{1}{2}|\alpha|^2} e^{\alpha a^\dagger} |0\rangle, \tag{B.3}$$

where we used $(a^\dagger)^n|0\rangle = \sqrt{n!}|n\rangle$. From equation (B.3) we can easily see that

$$P(n) = |\langle n|\alpha\rangle|^2 = \frac{e^{-\frac{1}{2}|\alpha|^2}(|\alpha|^2)^n}{n!}, \quad (\text{B.4})$$

which shows that coherent states have a Poisson distribution over number states. As mentioned earlier, coherent states are not orthogonal

$$\langle\alpha|\beta\rangle = e^{-\frac{1}{2}(|\alpha|^2+|\beta|^2)+\beta\alpha^*}, \quad (\text{B.5a})$$

$$|\langle\alpha|\beta\rangle|^2 = e^{-|\alpha-\beta|^2}, \quad (\text{B.5b})$$

nor they are complete

$$\int |\alpha\rangle\langle\alpha| \frac{d^2\alpha}{\pi} = 1. \quad (\text{B.6})$$

Computing the average of position $\hat{q} = \sqrt{\frac{\hbar}{2m\omega_0}}(a^\dagger + a)$ and momentum $\hat{p} = i\sqrt{\frac{m\omega_0\hbar}{2}}(a^\dagger - a)$ on coherent states, we arrive at

$$\begin{aligned} \langle\hat{q}\rangle &= \sqrt{\frac{\hbar}{2m\omega_0}}(\alpha^* + \alpha), \\ \langle\hat{p}\rangle &= i\sqrt{\frac{m\omega_0\hbar}{2}}(\alpha^* - \alpha), \\ \langle\hat{q}^2\rangle &= \frac{\hbar}{2m\omega_0}(\alpha^{*2} + \alpha^2 + 2\alpha\alpha^* + 1), \\ \langle\hat{p}^2\rangle &= -\frac{m\omega_0\hbar}{2}(\alpha^{*2} + \alpha^2 - 2\alpha^*\alpha - 1). \end{aligned}$$

Therefore

$$(\Delta\hat{q})^2 = \frac{\hbar}{2m\omega_0}, \quad (\text{B.7a})$$

and

$$(\Delta\hat{p})^2 = \frac{m\omega_0\hbar}{2}. \quad (\text{B.7b})$$

We find that the coherent states are in fact minimum uncertainty states

$$(\Delta\hat{q})(\Delta\hat{p}) = \frac{\hbar}{2}. \quad (\text{B.8})$$

We can rewrite α in terms of it's average on \hat{q} and \hat{p}

$$\alpha = \frac{1}{\sqrt{2m\omega_0\hbar}}[m\omega_0\langle\hat{q}\rangle + i\langle\hat{p}\rangle]. \quad (\text{B.9})$$

It can be shown that

$$|\alpha\rangle\langle\alpha|a = \left(\alpha + \frac{\partial}{\partial\alpha^*}\right)|\alpha\rangle\langle\alpha|, \quad (\text{B.10a})$$

and

$$a^\dagger|\alpha\rangle\langle\alpha| = \left(\alpha^* + \frac{\partial}{\partial\alpha}\right)|\alpha\rangle\langle\alpha|. \quad (\text{B.10b})$$

Appendix C

Classical Damping of an RLC Resonator

Assume that at $t = 0$, the following initial condition holds for the circuit of Figure C.1

$$i_L(0) = I_0, \tag{C.1a}$$

$$i'(0) = \frac{1}{L}v(0) = \frac{V_0}{L}. \tag{C.1b}$$

Therefore, the circuit's initial energy is $E_0 \equiv \frac{1}{2}CV_0^2 + \frac{1}{2}LI_0^2$. From the KVL and KCL, one can readily write

$$i_C + i_L + i_R = 0, \tag{C.2a}$$

$$i_C = C\frac{dv}{dt}, \tag{C.2b}$$

$$i_R = \frac{1}{R}v, \tag{C.2c}$$

$$v = L\frac{di_L}{dt}. \tag{C.2d}$$

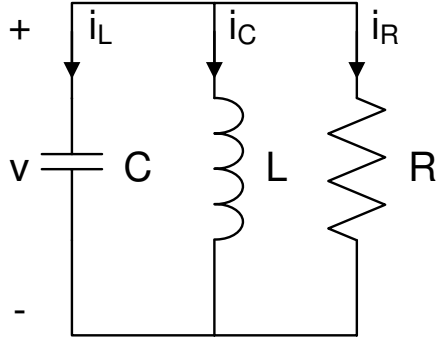


Figure C.1: A parallel RLC circuit.

Thus,

$$\frac{d^2}{dt^2}i_L + \frac{1}{RC} \frac{d}{dt}i_L + \frac{1}{LC}i_L = 0. \quad (\text{C.3})$$

Defining $\eta \equiv \frac{1}{RC}$ and $\omega_0^2 = \frac{1}{LC}$ and taking the Laplace transform,

$$S^2 I_L(S) - S I_0 - \frac{V_0}{L} + \eta S I_L(S) - \eta I_0 + \omega_0^2 I_L(S) = 0. \quad (\text{C.4})$$

Thus,

$$I_L(S) = \frac{S I_0 + (\eta I_0 + \frac{V_0}{L})}{S^2 + \eta S + \omega_0^2}. \quad (\text{C.5})$$

We may write equation (C.5) in the form

$$I_L(S) = \frac{S I_0 + (\eta I_0 + \frac{V_0}{L})}{(S + \eta/2)^2 + \Omega^2}, \quad (\text{C.6})$$

where

$$\Omega^2 \equiv \omega_0^2 - \eta^2/4. \quad (\text{C.7})$$

In case $\Omega^2 > 0$ (under-damped oscillation),

$$i_L(t) = I_0 e^{-\eta t/2} \left[\cos(\Omega t) + \frac{(\eta/2 + V_0/I_0 L)}{\Omega} \sin(\Omega t) \right]. \quad (\text{C.8})$$

If we define

$$\tan \phi = \left(\eta/2 + \frac{V_0}{I_0 L} \right) / \Omega, \quad (\text{C.9})$$

then

$$i_L(t) = I_0 e^{-\eta t/2} \cos(\Omega t - \phi). \quad (\text{C.10})$$

If $\Omega^2 = 0$ (critically-damped oscillation),

$$i_L(t) = I_0 e^{-\eta t/2} \left[1 + \left(\eta/2 + \frac{V_0}{L I_0} \right) t \right]. \quad (\text{C.11})$$

In case $\Omega^2 < 0$ (over damped oscillation),

$$i_L(t) = I_0 e^{-\eta t/2} \left[\left(\frac{1}{2} - \frac{\eta}{4|\Omega|} - \frac{V_0}{2L I_0 |\Omega|} \right) e^{-|\Omega|t} + \left(\frac{1}{2} + \frac{\eta}{4|\Omega|} + \frac{V_0}{2L I_0 |\Omega|} \right) e^{+|\Omega|t} \right]. \quad (\text{C.12})$$

Figure C.2 illustrates these responses for an RLC circuit with different R.

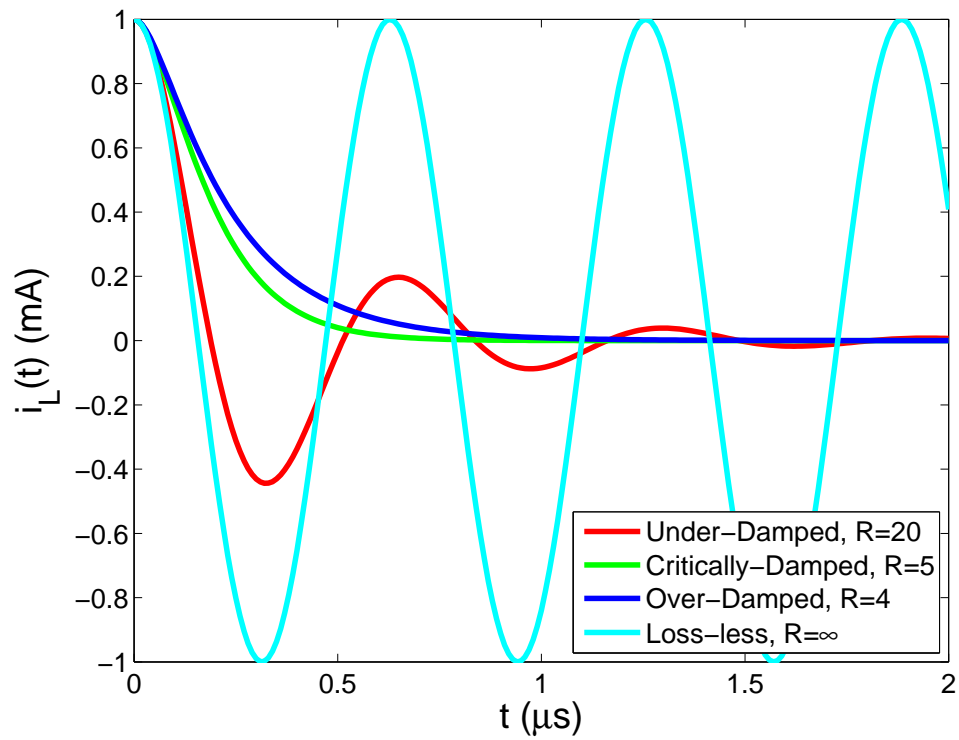


Figure C.2: Classical damping of a parallel RLC resonator with $L=1\mu\text{H}$, $C=10\text{nF}$, and $\omega_0=10$ Mrad/s.

Appendix D

Density Matrix of a Harmonic Oscillator

For a system with a Hamiltonian H at a temperature T [9],

$$\hat{\rho} = \frac{\exp(-H/k_B T)}{\text{Tr}[\exp(-H/k_B T)]}. \quad (\text{D.1})$$

We first evaluate the numerator with $H = \hbar\omega(a^\dagger a + \frac{1}{2})$.

$$\begin{aligned} e^{-\hat{H}/k_B T} &= \sum_m \left(\frac{-\hbar\omega(a^\dagger a + \frac{1}{2})}{k_B T} \right)^m \frac{1}{m!} \\ &= \sum_{n, m} n, m \frac{1}{m!} \left(\frac{-\hbar\omega}{k_B T} \right) (a^\dagger a + \frac{1}{2})^m |n\rangle\langle n| \\ &= \sum_{n, m} n, m \frac{1}{m!} \left(\frac{-\hbar\omega}{k_B T} \right) (n + \frac{1}{2})^m |n\rangle\langle n| \\ &= \exp\left(\frac{-\hbar\omega(n + \frac{1}{2})}{k_B T} \right) |n\rangle\langle n|. \end{aligned}$$

Now we calculate the trace,

$$\begin{aligned}\mathrm{Tr} \left(e^{-\frac{\hat{H}}{k_B T}} \right) &= \sum_n e^{-\frac{\hbar\omega(n + \frac{1}{2})}{k_B T}} \\ &= \frac{e^{-\frac{\hbar\omega}{2k_B T}}}{1 - e^{-\frac{\hbar\omega}{k_B T}}},\end{aligned}\tag{D.2}$$

and hence

$$\rho = \sum_n \left[1 - \exp\left(-\frac{\hbar\omega}{k_B T}\right) \right] \exp\left(-\frac{n\hbar\omega}{k_B T}\right) |n\rangle\langle n|.\tag{D.3}$$

Therefore,

$$\begin{aligned}\langle n \rangle &= \mathrm{Tr}(a^\dagger a \rho) = \sum_n \left(1 - e^{-\frac{\hbar\omega}{k_B T}} \right) n \exp\left(-\frac{n\hbar\omega}{k_B T}\right), \\ &= \left(1 - e^{-\frac{\hbar\omega}{k_B T}} \right) \frac{d \left(\frac{1}{1 - e^{-\frac{\hbar\omega}{k_B T}}} \right)}{d \left(-\frac{\hbar\omega}{k_B T} \right)}, \\ &= \frac{e^{-\frac{\hbar\omega}{k_B T}}}{1 - e^{-\frac{\hbar\omega}{k_B T}}} = \frac{1}{e^{-\frac{\hbar\omega}{k_B T}} - 1}.\end{aligned}\tag{D.4}$$

Thus,

$$e^{-\frac{\hbar\omega}{k_B T}} = \frac{\langle n \rangle}{\langle n \rangle + 1},\tag{D.5}$$

and

$$\rho = \sum_n \frac{\langle n \rangle^n}{[1 + \langle n \rangle]^{n+1}} |n\rangle \langle n|. \quad (\text{D.6})$$